The End-to-End BER Analysis of Two Simulated OFDM-RoF Systems

by

Wanzong Liu

A thesis
presented to the University of Waterloo
in fulfillment of the
thesis requirement for the degree of
Master of Applied Science
in
Electrical and Computer Engineering

Waterloo, Ontario, Canada, 2015

Author's Declaration

I hereby declare that I am the sole author of this thesis. This is a true copy of the thesis, including any required final revisions, as accepted by my examiners.

I understand that my thesis may be made electronically available to the public.

Abstract

With the rapid grown of informational and visual services, larger capacity and higher-speed transmissions are demanded in today's cellular network, which makes the current wireless networks eventually fail to deal with the growing total traffic. As a result, the way of achieving large capacity and high-speed transmission has undoubtedly been a critical task for the next generation mobile service carriers.

Radio-over-fiber (RoF) is one of the promising solutions to the exploding traffic, which can incorporate with Orthogonal Frequency Division Multiplexing (OFDM), namely OFDM-RoF, to resolve the capacity thirst with relatively lower cost.

In this thesis, two OFDM-RoF systems under different transmission schemes are studied regarding their end-to-end bit-error-rate (BER) performances. Particularly, a baseband OFDM-RoF system is simulated and analyzed by Matlab, where the nonlinear effect of the MZM transfer function will be focused in the first system, while the BER performance of the optical transmission line under various laser powers and fiber lengths will be considered in the second. Finally, the BER of the two systems are compared under different M-QAM modulations.

Acknowledgements

I would like to thank my supervisor Prof. Pin-Han Ho for the guidance and support throughout my time as a graduate student in University of Waterloo. It is his supervision and encouragement that help me complete this thesis.I would like to thank my co-supervisor Prof. Hamed Majedi for the help and advices with my thesis. Last but not the least, I am thankful to all my friends in Waterloo for their companion.

Dedication

To my parents, for their never-ending love and support.

Table of Contents

List of Tables

List of Figures

Chapter 1

Introduction

1.1 Motivation

Radio-over-fiber (RoF) is one of the promising solutions to deal with growing Internet traffic on the wireless mobile systems. By incorporating Orthogonal Frequency Division Multiplexing (OFDM) and the electro-optic device Mach-Zehnder modulators (MZMs), OFDM-RoF has been considered the next-generation wireless access technology that enabling cost effective bandwidth provisioning.

Previous studies on bit-error-rate (BER) analysis mostly focus on the effect of MZM on the optical fiber link [5]. In this thesis, we go one step further by investigating two OFDM-RoF transmission scenarios, where the end-to-end BER performance of OFDM-RoF system is simulated and analyzed. In the first scenario, the study focuses on the nonlinear effect of the MZM transfer function utilizing Matlab, while in the second, a different transmission scheme is implemented using a commercial software package, Optisystem, where the BER performance of the optical link is simulated under different Laser powers and fiber lengths. Finally, the BER of the two systems are compared under various M-QAM modulations.

1.2 Techniques

To achieve large capacity and high data rate, straightforward methods include reduction of cell sizes and exploration of unused bandwidths such as millimeter wave (mm-wave) frequencies. However, considering the installation and maintenance of the network infrastructure, these solutions may lead to extraordinarily high cost. Radio-over fiber (RoF) has

been considered a promising approach that can achieve high-speed transmissions at very low cost provided with the existing fiber backbone infrastructure [13] [21].

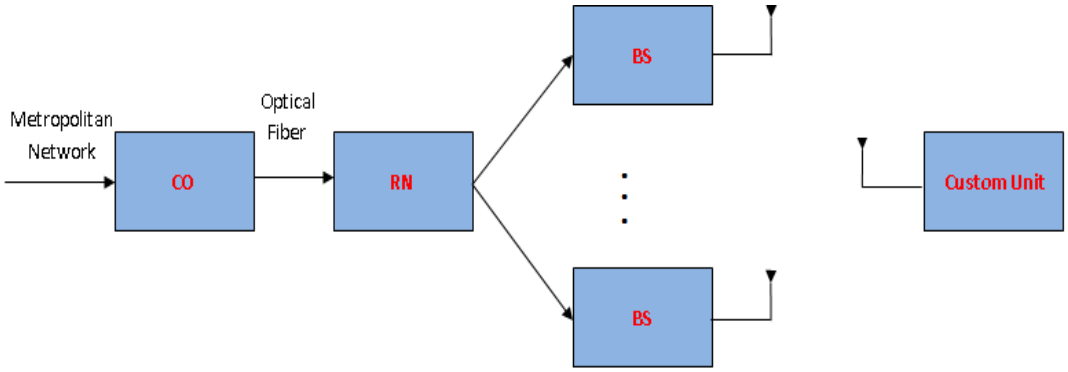

Figure 1.1: System diagram for Radio-over-fiber (RoF)

Fig. 1.1 shows a general architecture of RoF. the central office (CO) works as the gateway to the optical metropolitan backbone formed by the RoF and also serves a large number of widely distributed antenna base stations (BSs) and remote nodes (RNs). Low-cost optical backbone will be utilized to reduce the cost in the transmission to BSs.

Another issue is that the fiber dispersion will cause some non-linearity problems when applying fiber in transmission. Recently, the concept of Orthogonal Frequency Division Multiplexing (OFDM) has been applied to reduce the effect of dispersion in high-speed optical communication systems [26]. OFDM is one of the multicarrier modulation forms, using a number of harmonically related narrowband subcarriers to transmit a single high-speed information bearing stream [7]. By incorporating with Mach-Zehnder modulators (MZMs), the optical OFDM transmission system can achieve the lowest optical loss and the highest optical power handling capability. Applying such techniques, the OFDM-RoF system will have advantages in high speed transmission.

1.3 Organization

The thesis is organized as follows: Chapter 1 is an introduction; Chapter 2 provides essential background of Radio-over-fiber, OFDM-RoF systems and Mach-Zehnder modulators;

Chapter 3 provides an end-to-end BER analysis of a baseband OFDM-RoF system over Rayleigh fading channel; Chapter 4 presents a simulation of an analog OFDM-RoF system design by Optisystem, and the end-to-end BER of the system is also studied. Finally, the conclusions and discussions are given in Chapter 5.

Chapter 2

Background review

This chapter provides the background of Radio-over-fiber (RoF), Orthogonal Frequency Division Multiplexing (OFDM) RoF systems, and Mach-Zehnder Modulator (MZM).

2.1 Radio-over-fiber (RoF)

The radio-over-fiber (RoF) technology serves as a cost-effective last-mile access approach for the next generation radio access networks (RANs) [12]. It aims to save the operation and infrastructure cost by sharing common optical communication backbone with other carriers. Fig. 2.1 shows the structure of a typical RoF system that integrates both optical and wireless access networks via a common unified backbone [17]. The base stations (BSs) can be either traditional BS or simply a remote antenna unit, by which the management complexity can be minimized.

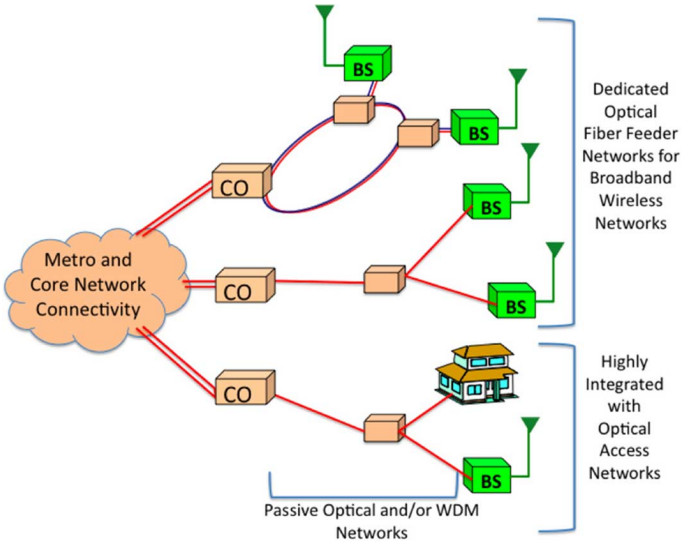

Figure 2.1: An illustration of an RoF access system [17]

In the RoF transmission systems, the electrical signal can be modulated onto the optical carrier by using either direct or external modulation and transmitted over the optical fiber. There are generally three transmission schemes of the fiber-wireless network based on the types of the transmitted electrical signal, which are baseband (BB) signal, analog radio frequency signal (analog RF) and digitized radio frequency signal (digitized RF) transmission over fiber.

Because of the nonlinearity fact of the transmitter and the chromatic dispersion over fiber, the analog RF signal (Fig. 2.2a) is subject to limited dynamic range, and this problem becomes more severe at higher RF carrier frequencies. In the second case of using BB over the fiber transmission (Fig. 2.2b), the problem of dispersion could be less significant at the expense of higher complexity in processing the baseband signals. In the third scheme as shown in Fig. 2.2c, the analog RF signal is digitized by bandpass sampling before launched in optical fiber in order to make the signal less sensitive to fiber dispersion [24].

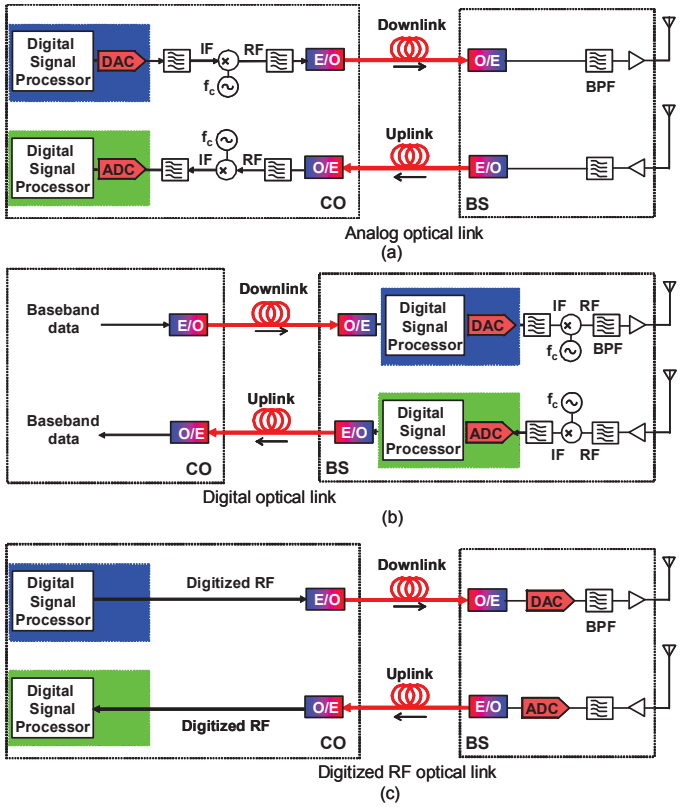

Figure 2.2: Transmission schemes of (a) Analog RoF (b) BB over fiber (c) Digitized RoF [13]

Based on these transmission schemes, a large number of researches in RoF systems have focused on improving the system performance by applying innovation techniques or devices. T.Van studied an RoF system with EDFA and a coherent receiver. The transmission length and signal quality can be significantly improved by implementing EDFA-Coherent detection [21]. Results show that digitized RoF transmission can realize better performance and higher linearity comparing to the analog RoF link, and increase system efficiency in terms of longer transmission distance, lower received optical power, and simpler BS structure [25]. Other modulation techniques such as optical-single-sideband-with-carrier (OSSB+C) are proposed to overcome the chromatic dispersion of fiber [20]. Note that all the above studies focused on the performance of the optical link, while the end-to-to-end BER with regard to the RF channel has never been considered.

2.2 Orthogonal Frequency Division Multiplexing (OFDM) RoF systems

Despite the convenience and simplicity, the RoF system suffers from the fiber dispersion problems, while Orthogonal Frequency Division Multiplexing (OFDM) is capable of dealing with the fiber dispersion [6]. By incorporating OFDM with RoF, the OFDM-RoF system is superior in spectrum utilization and resistance of Intersymbol Interference (ISI).

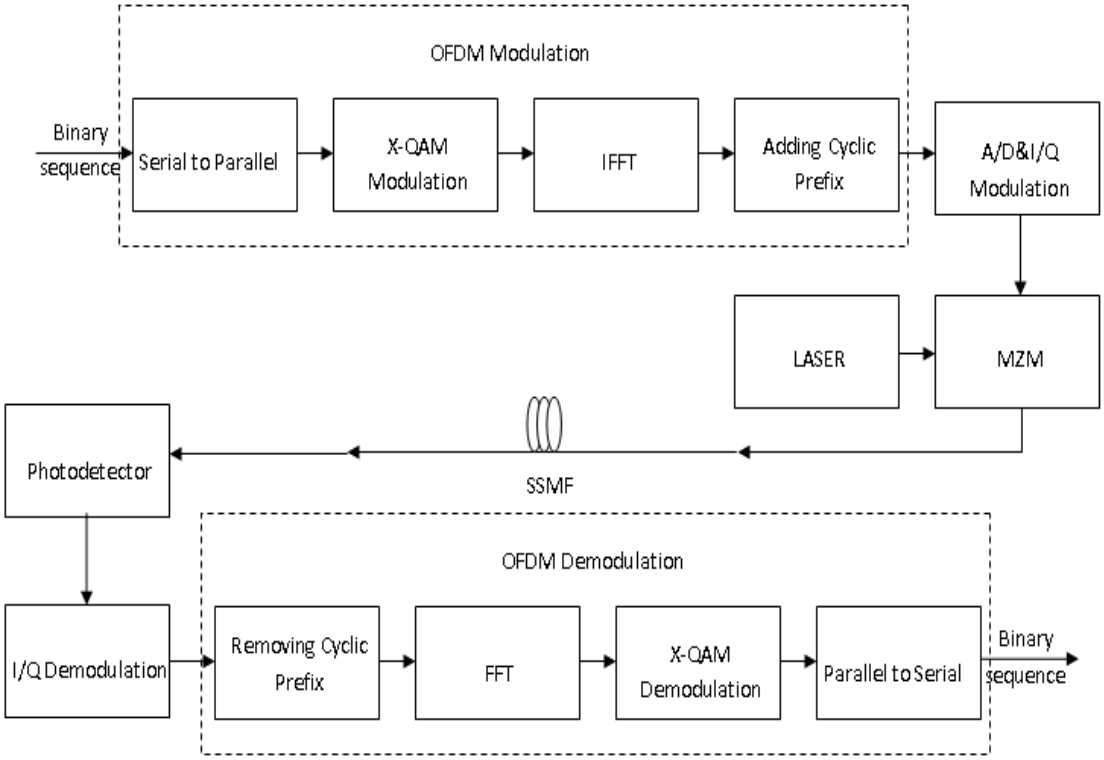

Figure 2.3: The block diagram of the OFDM-RoF system

Fig. 2.3 shows the block diagram of an OFDM-RoF system. It can be divided into several functional blocks, including OFDM modulator, the fiber-optic transmission and OFDM demodulator. Compared with using general FDM signals, the OFDM signal is transmitted over the fiber to reduce the effect of fiber dispersion.

Extensive research efforts have been addressed on the OFDM-RoF systems. Rao *et al.* investigated its BER performance by using different types of fiber, such as single mode

fiber (SMF) and dispersion compensated fiber (DCF) [18]. To handle the phase noise and nonlinear distortion of the OFDM-RoF systems, C. Wei, *et al.* established an experimental set-up of long-reach OFDM-RoF system at 60 GHz, where the phase noise compensation and bit-loading algorithms are employed [23]. A. Islam *et al.* investigated the OFDM-RoF link regarding its nonlinear performance and found that the OFDM-RoF system is less sensitive to the non-linear distortion of Mach-Zehnder modulator than that with the conventional single-carrier RoF system [10].

It is clear that the nonlinear effect of MZM critically limits the overall BER performance of the system [3], which will be further detailed in the next section.

2.3 Mach-Zehnder Modulator

Direct modulation of the laser sources is the simplest way of intensity modulation. However, the relative intensity noise (RIN) and distortions raise sharply when the modulation frequency reaches up to the relaxation resonance frequency of a semiconductor laser. Besides, direct modulation falls short in the case of long-distance transmission due to the large frequency chirp, especially for digital applications. Mach-Zehnder Modulators (MZMs), which serve as the most cost-effective and low-complexity external modulation approach in optical communications, can resolve the situation thanks to their lowest optical loss and the highest optical power handling capability. Fig. 2.4 shows the procedure of external modulation, where a constant-amplitude light signal is launched in an external modulator from the optical source, and the output signal of the modulator is a time-varying optical signal in a linear relation with the electrical driving signal.

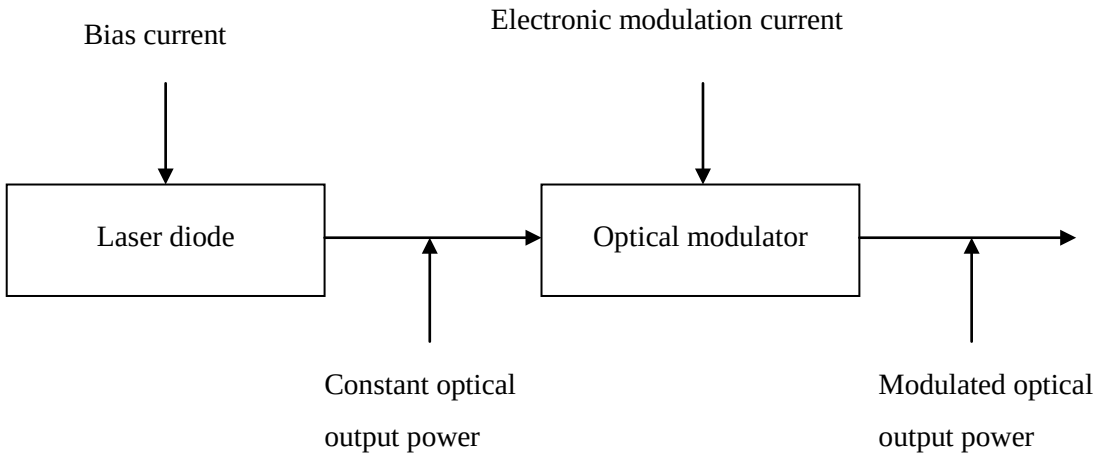

Figure 2.4: External modulation of a Laser diode

The optical property of a dielectric material can be changed by an electro-optic effect due to the presence of a static or low-frequency electric field. Electro-optic (EO) effect is the fact that the optical refractive index is changed in nonlinear optical (NLO) crystals in the presence of electric field. Currently, $LiNbO_3$ is one of the most widely used materials for the electro-optic devices manufacturing. Optical waveguides made of $LiNbO_3$ are generally superior in high EO coefficient, low optical loss and high optical coupling efficiency with single-mode optical fiber.

To make use of EO effect, the change of optical refractive index results in the difference in optical phase, which can be converted into intensity modulation in a MachZehnder interferometer [11].

MZM is a class of guided-wave electro-optic phase modulators, which can be utilized to build up waveguide interferometers for effective amplitude modulation of guided optical waves, which means that the transfer function of the MZM is the output optical power with respect to the applied voltage. A Mach-Zehnder waveguide interferometer is made up of two parallel waveguides connected at the input and output ends. The two waveguides are generally connected by beam-splitting and beam-combining optical couplers. One of the typical couplers is a Y-junction waveguide, which is shown in Fig. 2.5.

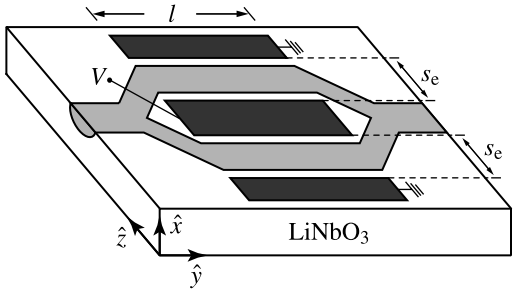

Figure 2.5: The layout of a Y-junction MZM [15]

The input optical signal is divided into two equal portions at its optical input port by using an optical splitter. The two separate waveguides are often known as two arms of MZM to propagate the split signal [15]. In an MZM, one or both of these waveguides are designed as electro-optic (EO) waveguides. The optical phase is modulated by an applied voltage along the waveguides. The optical waves passing through the two arms are combined as a single mode near the combiner resulting in a maximum intensity output when these two are in phase, or as a higher order spatial mode, resulting in a minimum intensity output when these two are out of phase, where most part of the optical output will become an unguided wave.

The output optical field amplitude of the MZM is given by the Eq. (2.1)

$$A_{out} = \frac{\sqrt{2}}{2}(A_1 e^{j\Phi_1} + A_2 e^{j\Phi_2}) \tag{2.1}$$

where A_1 and A_2 are the input optical amplitudes in the two arms, respectively, $A_1^2 + A_2^2$ is the total optical input power P_{in}, and Φ_1 and Φ_2 are the optical phase delays of the two arms.

$$P_{in} = A_1^2 + A_2^2 \tag{2.2}$$

The output optical power can be calculated as Eq. (2.3):

$$P_{out} = |A_{out}|^2 = \frac{1}{2}[A_1^2 + A_2^2 + 2A_1A_2cos(\Phi_1 - \Phi_2)] \tag{2.3}$$

There are two parts of the phase difference: one is the phase difference at zero applied voltage; and the other is the phase difference caused by the applied voltage. When only one arm is modulated, the phase difference becomes:

$$\Delta\Phi = \gamma\Delta n\frac{2\pi}{\lambda}L \tag{2.4}$$

where Δn is the optical index change in the active layer of the waveguide; γ is the optical confinement factor, which is the confined portion of optical mode in the active layer, $\gamma\Delta n$ is the index change for the optical mode; λ is the optical wavelength; L is the modulation length. If both of the two arms are modulated in a pushpull mode, where the phase changes in the two arms are opposite to each other, the overall phase change $\Delta\Phi$ is doubled. If the modulation is based on the EO effect, then

$$\Delta n = \frac{1}{2}n_0^3 r_{ij}\frac{V}{d} \tag{2.5}$$

Where n_0 is the optical index of the active layer at zero applied voltage; r_{ij} is the relevant EO coefficient, which is relevant to the material, optical polarization and electrode design; V is the applied voltage; d is the spatial gap between the electrodes where the voltage V is applied. We can get the Eq. (2.6) and (2.7) by combining these equations:

$$\Delta\Phi = \frac{\pi}{\lambda}n_0^3 r_{ij}\frac{\gamma L}{d} = \frac{\pi V}{V_\pi} \tag{2.6}$$

and

$$V_\pi = \frac{\lambda}{n_0^3 r_{ij}}\frac{d}{\gamma L} \tag{2.7}$$

V_π is the electrical voltage value at which the phase shift induced by voltage reaches π or 180°. It is a very important parameter for the MZM, as it determines the linear region of the MZM.

The transfer function of MZM is given by Eq. (2.8) [16]

$$E_{out} = (\frac{1}{2}e^{j\frac{\pi V_a}{2V_\pi}} + \frac{\gamma}{2}e^{j\frac{\pi V_b}{2V_\pi}})E_{in} \tag{2.8}$$

where E_{out} is the output field of MZM; E_{in} is the input optical field; V_a and V_b are applied electrical voltages which are related to the input data; $\gamma \in [0, 1]$ is the imperfectness parameter of MZM, and it is the parameter about the imbalance of the two arms of MZM.

As the MZM is in a push-pull configuration with a differential input data ($V_a = -V_b$), when $\gamma = 1$, the output optical field is a sinusoidal function as Eq. (2.9).

$$E_{out} = \cos(\frac{\pi V_a}{2V_\pi})E_{in} \tag{2.9}$$

Since the transfer function of MZM is not a linear function, the nonlinear distortion will occur when implementing MZM in the system.

Chapter 3

The end-to-end BER simulation of a baseband OFDM-RoF system

In this chapter, a baseband OFDM-RoF system is simulated and analyzed by Matlab, where the nonlinear effect of the MZM transfer function will be focused. The end-to-end BER of the downlink system is calculated under different modulation schemes. The result analysis also compares the BER between external modulation scheme implementing the MZM and direct modulation scheme without the MZM.

3.1 The schematic model of the baseband OFDM-RoF system

The baseband OFDM-RoF system is described in Fig. 3.1. It can be seen that the system generally consists of several parts, i.e., OFDM modulation, optical link, HPA and RF channel and OFDM demodulation, where the OFDM signal is generated by the OFDM modulation part; the electric-to-optic (EO) conversion, fiber transmission and optic-to-electric (OE) conversion are done within the optical link part; the signal is then transformed by a high-power-amplifier (HPA) and broadcast over the Rayleigh fading channel. Finally, the received signal is demodulated by the OFDM demodulation part and BER of the system is calculated.

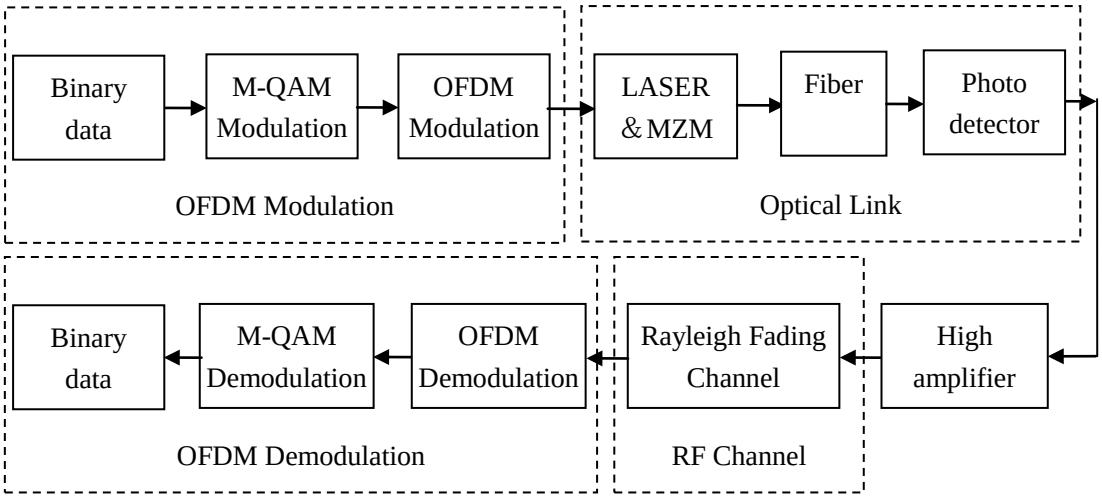

Figure 3.1: Transmission scheme of a baseband OFDM-RoF system

Fig. 3.2 depicts the detailed block diagram of the baseband OFDM-RoF system simulation, where the types of signal are identified between the blocks. The simulation build-up of each block is introduced in the following sections. Since the MZM is the only device that has a nonlinear transfer function, the MZM effect on the system BER performance is carefully examined.

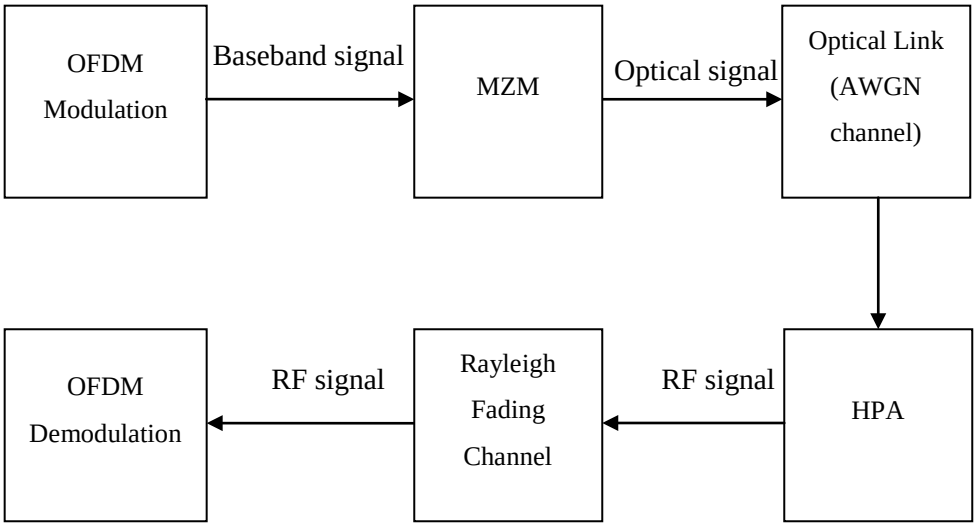

Figure 3.2: Block diagram of the baseband OFDM-RoF system simulation

3.2 OFDM Modulation

The original input data is generated by a random binary generator to form the original serial data vector, which has a total number of N. In order to make the serial binary data M-QAM modulated, the serial data vector is reshaped into an $m \times n$ matrix, where $N = m \times n$, and $m = \log_2 M$. When the symbols are BPSK modulated, this step can be skipped.

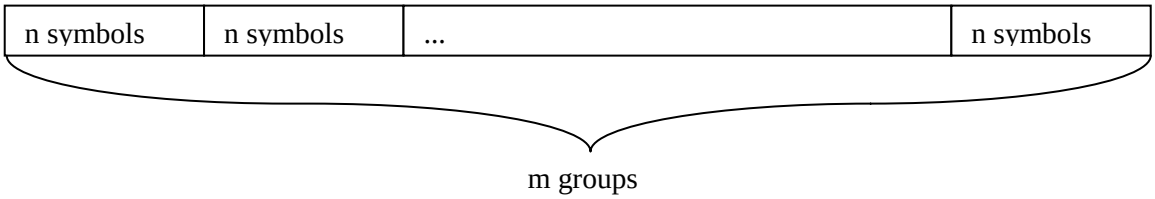

Figure 3.3: Regroup of the data

The next step is M-QAM modulation. The Quadrature Amplitude Modulation (QAM) involves both amplitude-shift and phase-shift keying, where the amplitude and phase of a

QAM signal are modulated as two independent parameters. The signal can be expressed as Eq. (3.1):

$$\begin{aligned} X_n(t) &= a(n)\cos(\omega_n t) + b(n)\sin(\omega_n t) \\ &= \gamma(n)\cos(\omega_n t + \psi_n) \end{aligned} \tag{3.1}$$

where

$$\gamma(n) = \sqrt{(a^2(n) + b^2(n))} \tag{3.2}$$

and

$$\Psi_n = \tan^{-1}\frac{b(n)}{a(n)} \qquad n = 0, 1, , N-1 \tag{3.3}$$

According to IEEE 802.11a standard [1], the regrouped binary symbols are M-QAM modulated. The bit-encoding constellation is shown in Fig. 3.4, and the bit-encoding table is presented in Table. 3.2, where b_0 is related to the I value in BPSK; for QPSK, b_0 is related to the I value and b_1 is related to the Q value; b_0b_1 is related to the I value and b_2b_3 is related to determines the Q value in 16-QAM; for 64-QAM, $b_0b_1b_2$ is related to the I value and $b_3b_4b_5$ is related to the Q value. The M-QAM encoding is performed according to the encoding table in Matlab simulation.

The QAM signal should be normalized according to the K_{MOD}. The signal $(I + jQ)$ value of a QAM signal is multiplied by the normalization factor K_{MOD}, as described in Eq. (3.4):

$$d = (I + jQ)K_{MOD} \tag{3.4}$$

The K_{MOD} factor is determined by Table. 3.1

Modulation	K_{MOD}
BPSK	1
QPSK	$1/\sqrt{2}$
16-QAM	$1/\sqrt{10}$
64-QAM	$1/\sqrt{42}$

Table 3.1: K_{MOD} factors of different modulation

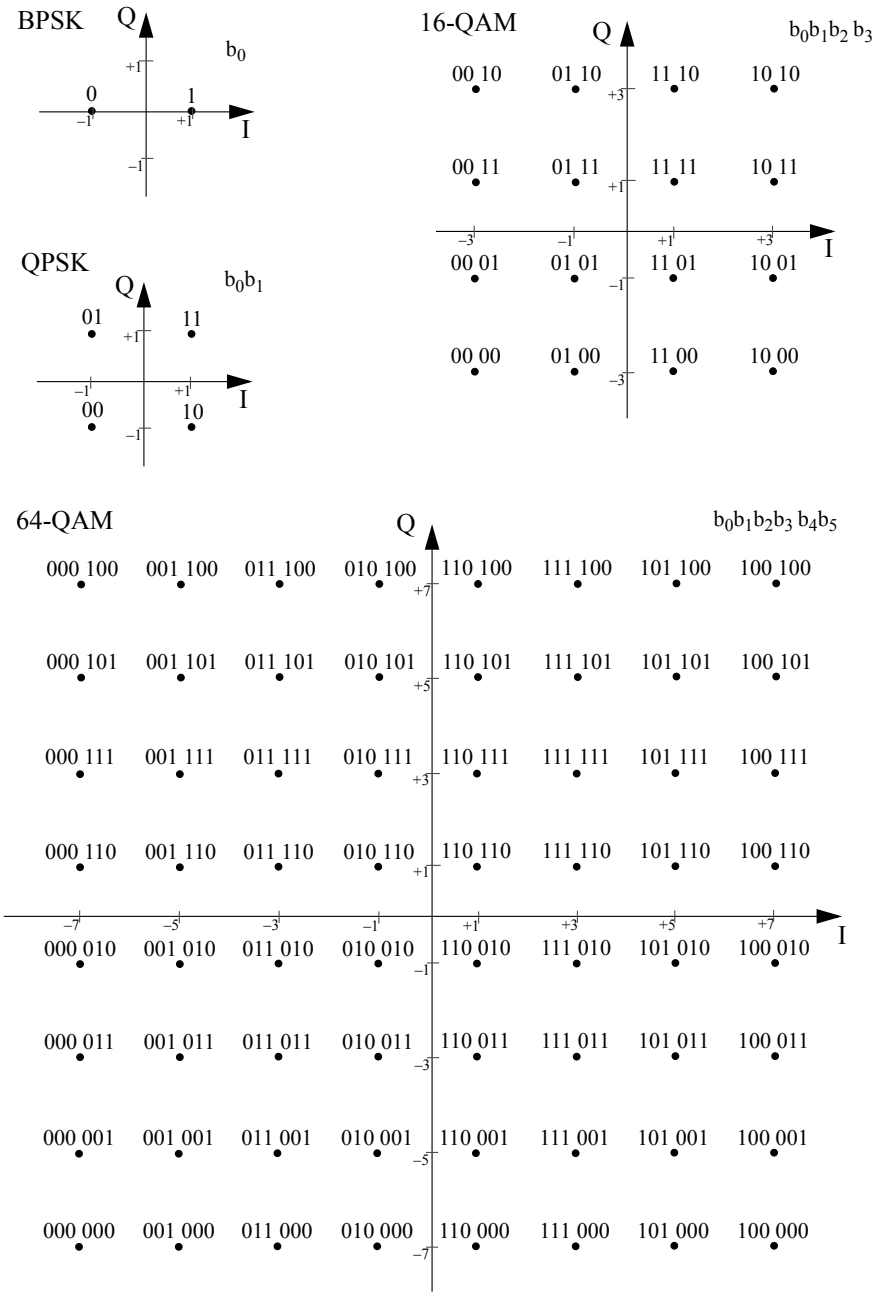

Figure 3.4: IEEE 802.11a Standard bit-encoding constellation of BPSK, 4-QAM, 16-QAM and 64-QAM [1]

BPSK encoding table

Input bit(b_0)	I-out	Q-out
0	-1	0
1	1	0

QPSK encoding table

Input bit(b_0)	I-out
0	-1
1	1

Input bit(b_1)	Q-out
0	-1
1	1

16-QAM encoding table

Input bit(b_0b_1)	I-out
00	-3
01	-1
11	1
10	3

Input bit(b_2 b_3)	Q-out
00	-3
01	-1
11	1
10	3

16-QAM encoding table

Input bit($b_0b_1b_2$)	I-out
000	-7
001	-5
011	-3
010	-1
110	1
111	3
101	5
100	7

Input bit($b_3b_4b_5$)	Q-out
000	-7
001	-5
011	-3
010	-1
110	1
111	3
101	5
100	7

Table 3.2: IEEE 802.11a Standard bit-encoding table

After the signal is QAM modulated, the signal is performed inverse discrete Fourier transform (IDFT) to be converted into the OFDM signal. The DFT and IDFT of signal $s(k), k = 0, 1, 2, ..., K-1$ is shown in Eq. (3.5) and (3.6), respectively:

$$S(n) = \frac{1}{\sqrt{K}} \sum_{k=0}^{K-1} s(k) e^{-j(2\pi/K)nk} \tag{3.5}$$

$$s(k) = \frac{1}{\sqrt{K}} \sum_{k=0}^{K-1} S(n) e^{j(2\pi/K)nk} \tag{3.6}$$

The OFDM signals are obtained after the IDFT progress.

3.3 Mach-Zehnder Modulator Transfer Function

The modulated OFDM signal is transformed by MZM with a transfer function given in Eq. (2.9). In this study, the bandwidth of MZM is assumed to be wider than the bandwidth of OFDM signal. The transfer function of MZM is plotted according to the Eq. (2.9) in Fig. 3.5, with a typical $V_\pi = 6V$ [15].

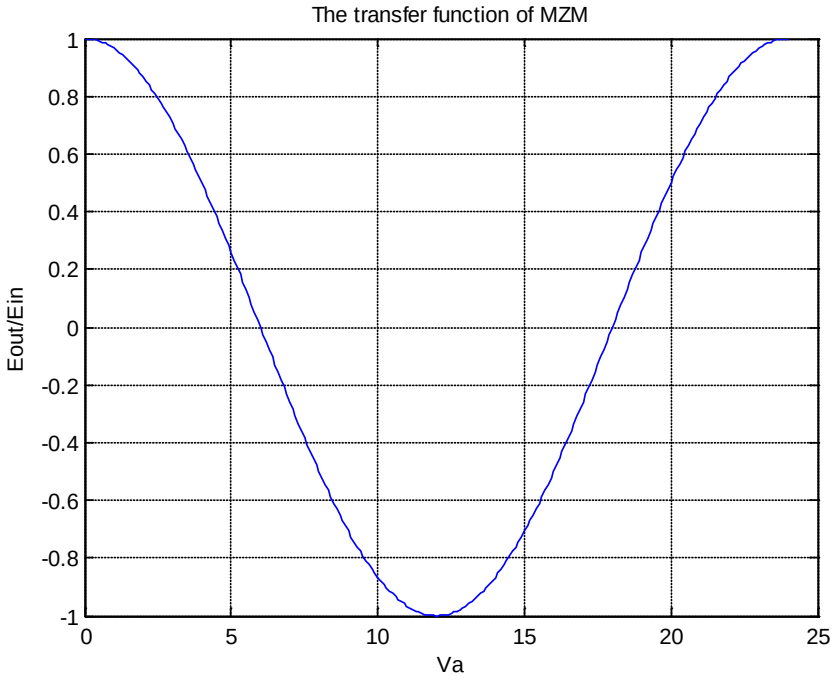

Figure 3.5: The transfer function of MZM ($V_\pi = 6V$)

Because of the cosine behavior of the function, the non-linear distortion may cause sharp increase in the bit-error-rate when the OFDM signal is MZM external modulated.

Bohara and Ting built up an equivalent polynomial model for non-linear power amplifiers [4], and this method can be used for the modeling of MZM as well. When ϕ_{bias} of this transfer function is $3\pi/2$, the baseband equivalent polynomial model for the output electrical field of the MZM is described with Eq. (3.7):

$$y_n = \sum_{k=1}^{K} a_k (x_n)^k, k - odd \tag{3.7}$$

where the discrete vector x_n is the applied voltage and y_n is the output of the MZM. n is the discrete time domain samples, a_k is the nonlinear odd coefficients, and k is the order of nonlinearity. A third order polynomial approximation of MZM, which is in the working region of $3V_\pi \pm V_\pi$, can be expressed by Eq. (3.8) [16]:

$$y_n = a_1 x_n + a_3 (x_n)^3 \tag{3.8}$$

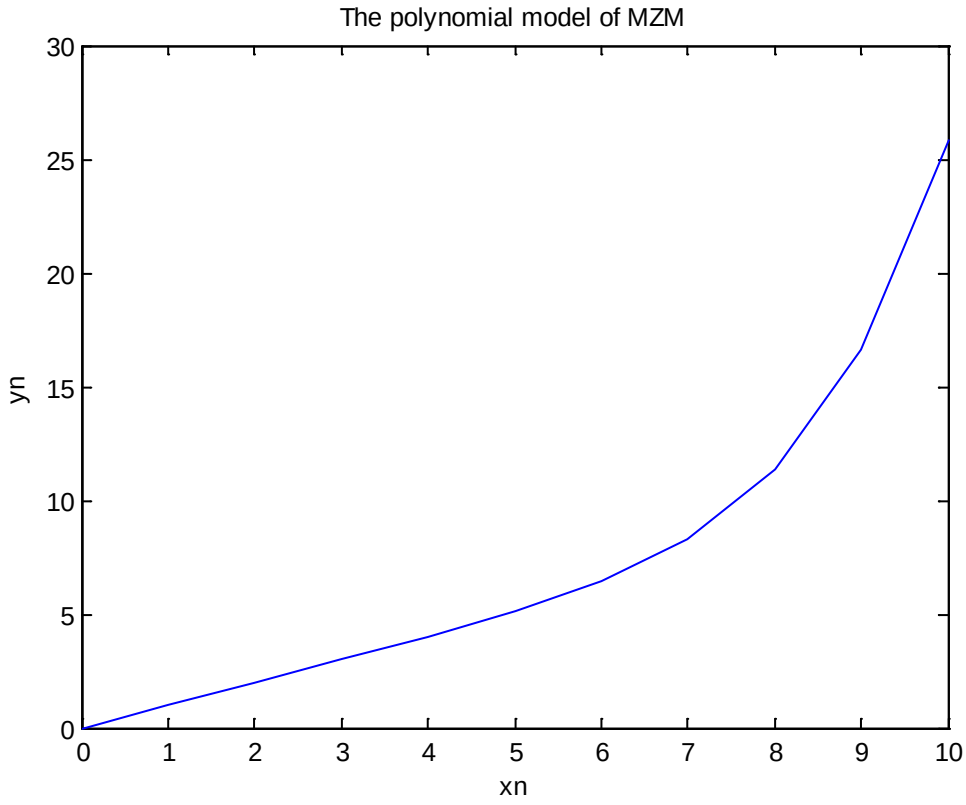

Figure 3.6: The polynomial model of MZM

The relation of x_n and y_n is shown in Fig. 3.6, which is used in Matlab simulation of MZM.

3.4 The rest of the optical link

The rest part of the optical link includes the single mode fiber and photodetector. Fig. 3.7 shows a typical transfer function of a photodetector, where the output voltage has a linear response versus the input optical power within the working region.

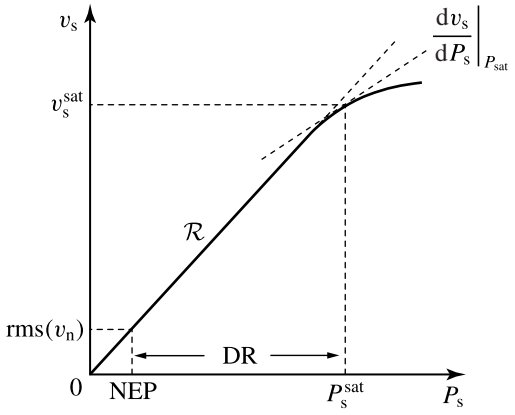

Figure 3.7: The response of a typical photodetector as a function of input optical power vs output voltage [15]

The attenuation and dispersion of a single mode fiber can be described by Eq. (3.9) and (3.10), respectively:

$$P_{out}(dBm) = P_{in}(dBm) - \alpha(dB \cdot km^{-1})L(km) \tag{3.9}$$

$$\sigma(ps) = D(ps \cdot km^{-1} \cdot nm^{-1})L(km)\lambda(nm) \tag{3.10}$$

The signal spread caused by the fiber dispersion is very small for 50 km fiber transmission distance after calculation and it has little effect on the baseband OFDM transmission, which is ignored in the simulation. The noise of the fiber can also be ignored compared with the noise of photodetector. Since the transfer function of photodetector is linear, the noise can be considered as a white Gaussian noise with an SNR defined in Eq. (3.11) [26]:

$$SNR_{PD} = R^2 P_{in}^2 / (\frac{4k_B T F_n \Delta f}{R_L} + 2qRP_{in}\Delta f) \tag{3.11}$$

where R is the responsivity of the photodetector, T is temperature, k_B is Boltzmann constant, q is the electric charge, R_L is the load resistor to convert output current to a voltage signal, $\Delta f = B_{DR}/2$ is the bandwidth, and F_n is the receiver noise figure. There is no nonlinear noise drawn from the fiber and the photodetector.

In conclusion, the rest of the optical link is modelled as an AWGN channel, whose SNR is mainly decided by the noise of photodetector.

3.5 HPA and Rayleigh fading channel

In order to clip the signal amplitude to an appropriate level, a soft limiter high power amplifier (HPA) is used ahead of the Rayleigh fading channel [14].The relation between the input signal $F(t) = x(t)e^{i\theta(t)}$ and the output signal $y(t)e^{i\theta(t)}$ can be expressed by Eq. (3.12):

$$y(t) = y = h(x) = \begin{cases} -A & if|x(t)| \leqq -A \\ x(t) & if|x(t)| < A \\ A & if|x(t)| \geqq A \end{cases} \tag{3.12}$$

where A and $-A$ is the clipping threshold of the HPA.

The signal is then broadcast over a Rayleigh fading channel, which is randomly delayed, reflected, scattered, and diffracted by buildings and obstacles. Multipath fading is composed of the constructive and destructive of these signal components, which can be modelled by the Rayleigh multipath fading channel [19].

For a Rayleigh distributed random variable, the average power can be described as:

$$\Omega = E[a^2] = 2\sigma^2 \tag{3.13}$$

In this case, the channel fading amplitude a is distributed according to

$$f_a(a) = \frac{2a}{\Omega} exp(\frac{-a^2}{\Omega}) \tag{3.14}$$

The channel response of Rayleigh fading is Gaussian progress with zero mean and variance of $\Omega/2$, which supported by Matlab.

3.6 OFDM Demodulation

The OFDM demodulation is the exact inverse operation of the OFDM modulation. Discrete Fourier Transform (DFT) is performed to reconstruct the M-QAM data after passing through the Rayleigh fading channel. The received data matrix is reshaped and demodulated by an M-QAM demodulator, and the decimal data is then reconverted to the binary data. The detailed progress is shown in Fig. 3.8.

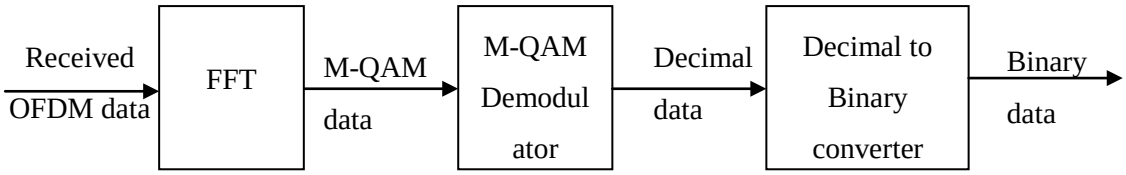

Figure 3.8: The OFDM Demodulation

3.7 Result analysis

Based on the simulation model described in the previous sections, the simulation steps are summarized as follows:

1. Generate original baseband signal with random binary generator.
2. Reshape the original data matrix and modulate into different modulation, i.e., BPSK, 4-QAM, 16-QAM, 64-QAM.
3. Perform IDFT to modulate into OFDM signal.
4. Change the signal using MZM and HPA applying their transfer functions.
5. Add an additive white Gaussian noise to the signal caused by the photodetector.
6. Transform the signal with the Rayleigh fading channel model.
7. Demodulate the received signal and calculate the BER.

The BER of the system is calculated by comparing the final data output data sequence with the original one, which is shown in the Eq. (3.15):

$$BER = \frac{n_{rr}}{N_{sym}} \tag{3.15}$$

where n_{rr} is the number of error symbol and N_{sym} is the total number of symbol transmitted.

E_b/N_0 is the energy per bit to noise power spectral density ratio. It is a normalized signal-to-noise ratio (SNR) measure, which is also known as the "SNR per bit". It can be used to compare the performance of different modulation schemes without taking bandwidth into consideration.

The theoretical BER of BPSK modulation scheme over Rayleigh fading channel is given by Eq. (3.16) [22]:

$$P_b = \frac{1}{2}(1 - \sqrt{\frac{E_b N_0}{1 + E_b N_0}}) \tag{3.16}$$

Fig. 3.9 shows both simulated and theoretical BER vs E_b/N_0 plot of the OFDM-RoF system using BPSK modulation over Rayleigh fading channel.

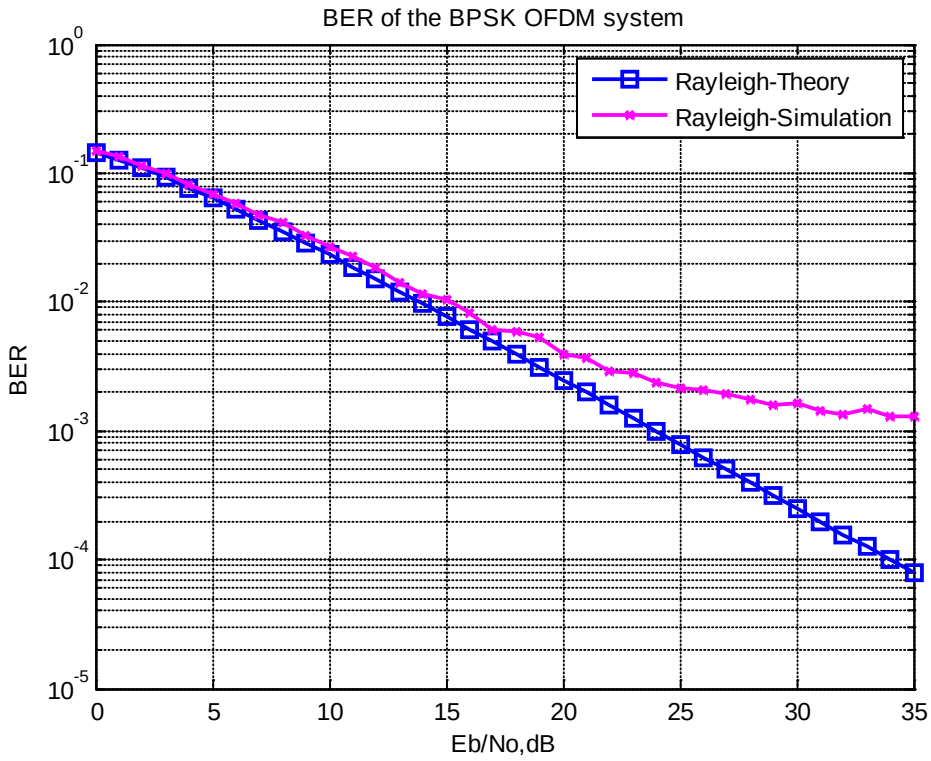

Figure 3.9: simulated and theoretical BER vs E_b/N_0 plot of the OFDM-RoF system using BPSK modulation over Rayleigh fading channel

As we can see from the figure, the simulated BER vs E_b/N_0 plot is different from the result of theoretical Rayleigh channel BER plot because of the white Gaussian noise of the optical link.

Although direct modulation has severe disadvantages in the high-speed transmission systems, it can be taken as a reference to examine how MZM will affect the BER of the system. In the direct modulation system, the MZM is not used and no nonlinear noise is introduced in electrical to optical conversion.

Fig. 3.10 displays the BER of BPSK, 4-QAM, 16-QAM and 64-QAM under external modulation with presence of MZM. And Fig. 3.11 displays the BER of BPSK, 4-QAM, 16-QAM and 64-QAM applying direct modulation without MZM.

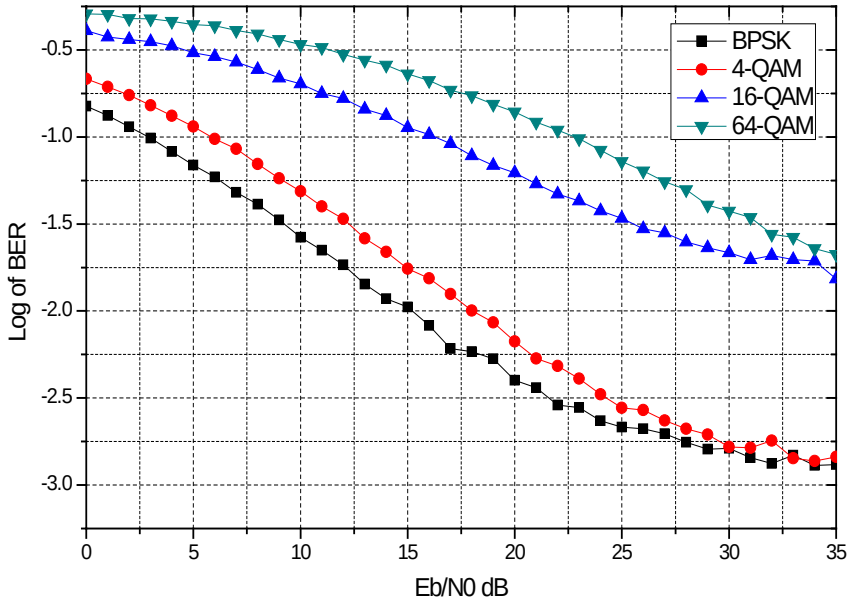

Figure 3.10: The BER of BPSK, 4-QAM, 16-QAM and 64-QAM using MZM as external modulator

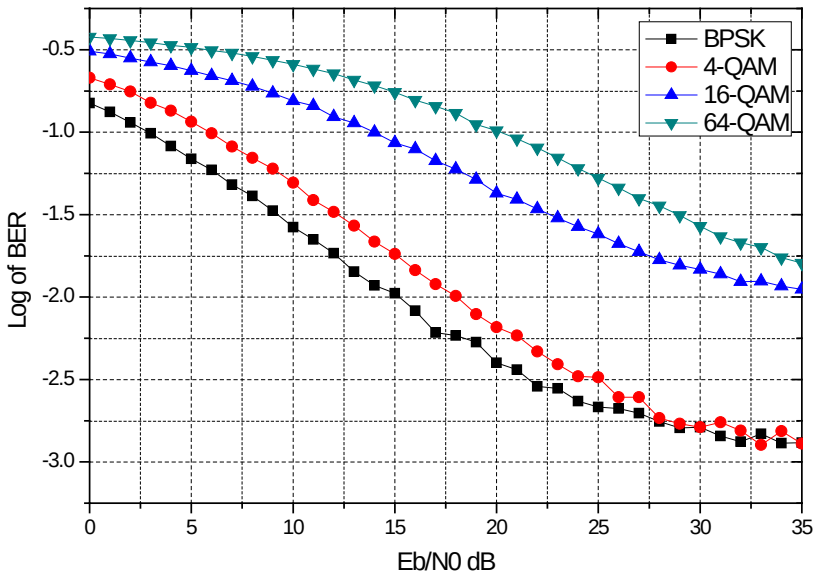

Figure 3.11: The BER of BPSK, 4-QAM, 16-QAM and 64-QAM using direct modulation without MZM

From Fig. 3.10 and 3.11, it can be concluded that the BER of the system is higher under higher level of M-QAM modulation. Fig. 3.12 compares the BER of a) BPSK, b) 64-QAM under direct modulation without MZM and external modulation with MZM.

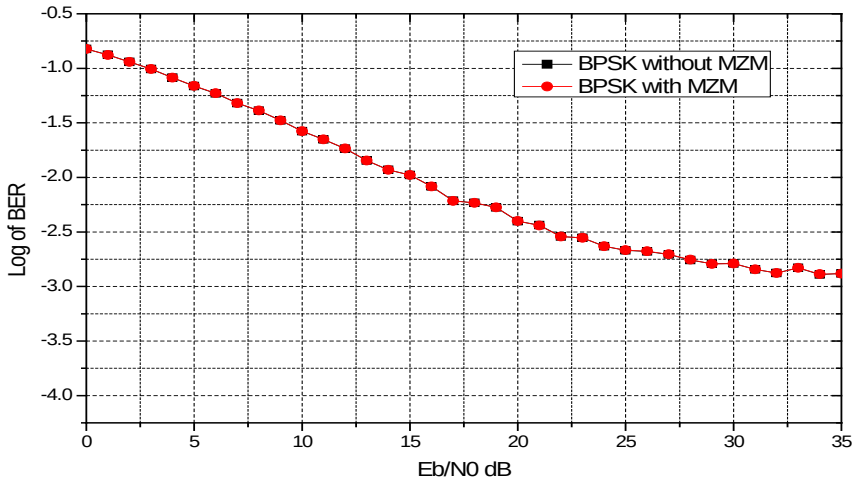

a)

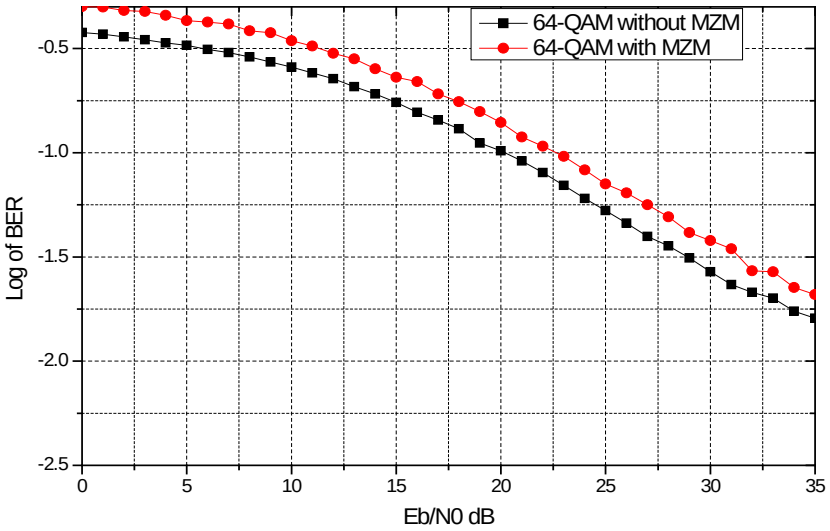

b)

Figure 3.12: The BER of a) BPSK, b) 64-QAM under direct modulation without MZM and external modulation with MZM

From above studies, we know that the BER performance of the system is worse under higher level of M-QAM modulation; MZM will introduce distortion to the system because

of the nonlinear part of its transfer function, and this effect is more obvious when M-QAM modulation is higher due to a greater peak-to-average power ratio (PAPR).

There are several potential ways to reduce the distortion that introduced by MZM. Linghui RAO, *et al.* [18] use electro-absorption modulator (EAM) to replace MZM in the system. However, the photocurrent generated by the electro-absorption may have effect on the modulator performance at high optical power. Y. London, *et al.* [16] applied pre-distortion technique before the MZM, which can artificially increase the linear region of the MZM, but may result in extremely low driving voltage when the peak power is high.

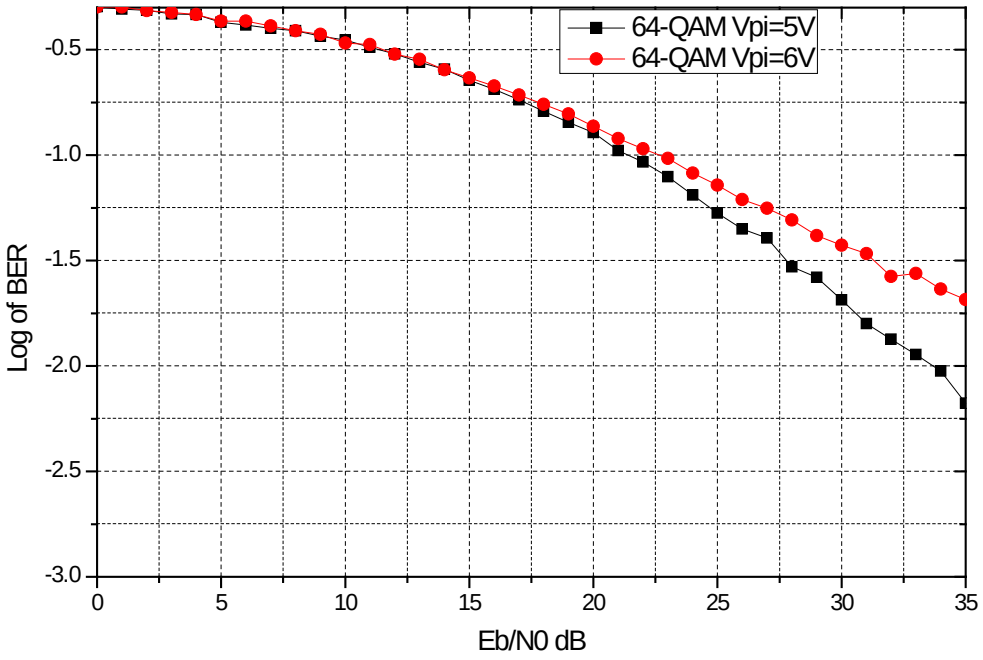

Figure 3.13: The BER of 64-QAM system with different V_π

From the studies of MZM, we know that V_π is a fixed parameter for a certain MZM, which is mainly determined by the material and chip size. In this thesis, the method of choosing MZM with different V_π is proposed. From Fig. 3.13, we know that a smaller V_π leads to a better BER performance of the system.

Chapter 4

The end-to-end BER analysis of the analog OFDM-RoF system

In this chapter, the end-to-end BER performance of an analog OFDM-RoF system is simulated and analyzed by incorporating a commercial software Optisystem and Matlab coding. The downlink BER of the optical link of the system is studied under various Laser powers and fiber transmission distances. The end-to-end BER of the baseband scheme system and the analog RF scheme system are compared at the end of the chapter.

4.1 The analog OFDM-RoF system build-up

An anlog RF OFDM-RoF system is built up to analyze the BER of the system. Fig. 4.1 presents the transmission diagram of the analog OFDM-RoF system. The simulation of the first half of the system, i.e. optical transmission part, is completed with the commercial software Optisystem, while the simulation of second half, i.e. RF channel part, is done utilizing Matlab coding. Ideally, the insertion module is not necessary in the actual system. However, there is no RF module available in the software package Optisystem. To co-simulate with Matlab, the error-free insertion module is added to build up a equivalent simulation system.

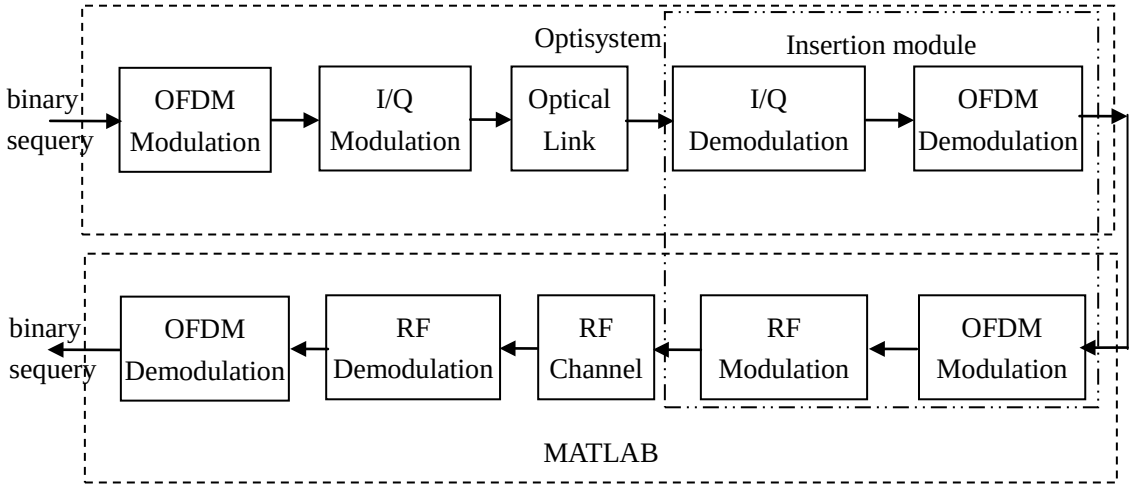

Figure 4.1: Simulation scheme for the analog OFDM-RoF system

To calculate the end-to-end BER of the system, the BER from the Optisystem is utilized to build a binary sequence with a BER_{opt}. This sequence with error is then OFDM modulated and transmitted over the Rayleigh fading channel. The end-to-end BER is calculated by comparing the demodulated data sequence with the error free original sequence.

The detailed structure and key parameters in each block are introduced in the following sections.

4.2 OFDM Modulation of the simulated system

The first half of the transmission system is completed with commercial software Optisystem. There are two simulation stereotypes of systems in the software according to the methods of demodulation: direct detection optical orthogonal frequency division multiplexing system and coherent detection orthogonal frequency division multiplexing system. As for the two systems, the coherent detection system surpasses in performance to direct detection system, but the structure of coherent detection system at the receiver end is much more complex; while the direct detection system is superior in simpler system structure. In this study, a direct-detection system is implemented due to its simplicity at the receiver end.

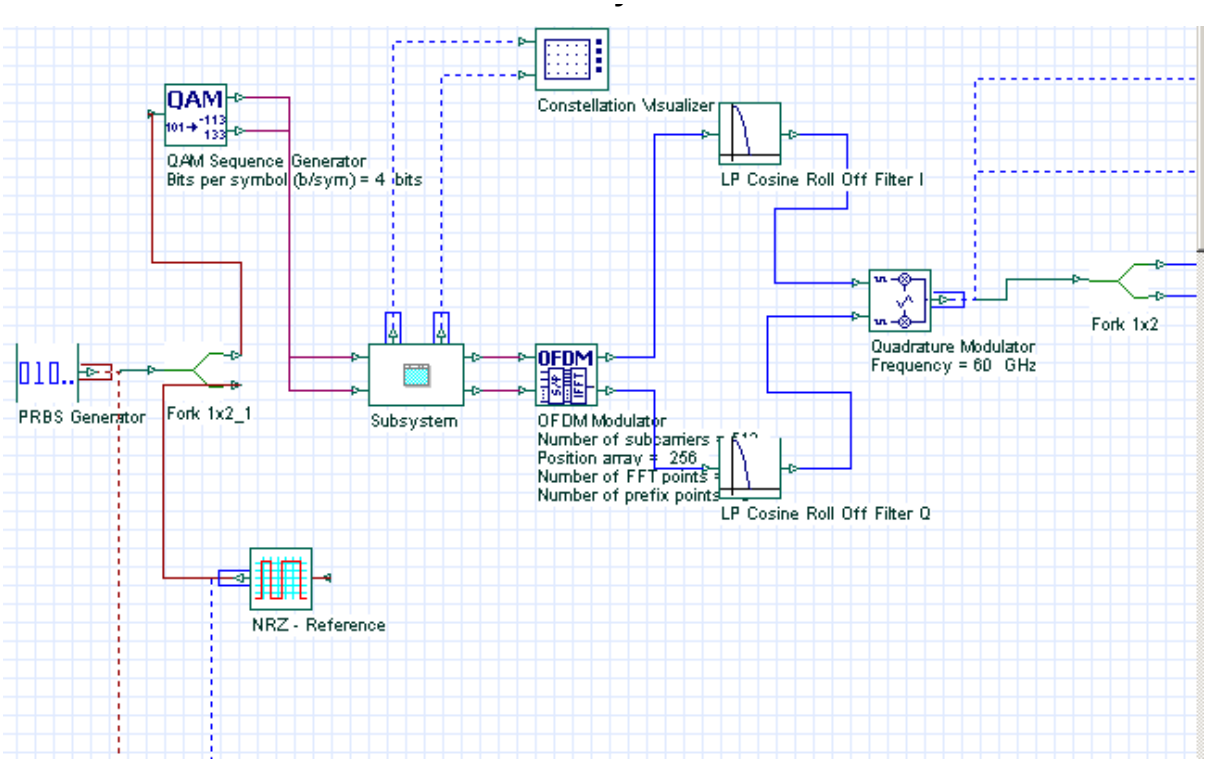

Figure 4.2: The OFDM Modulation scheme

According to the simulation diagram shown in Fig. 4.2, the OFDM modulation part of the OFDM-RoF system is established, where each block component works as a specific device in the system. Fig. 4.3 is the global parameter settings of the system.

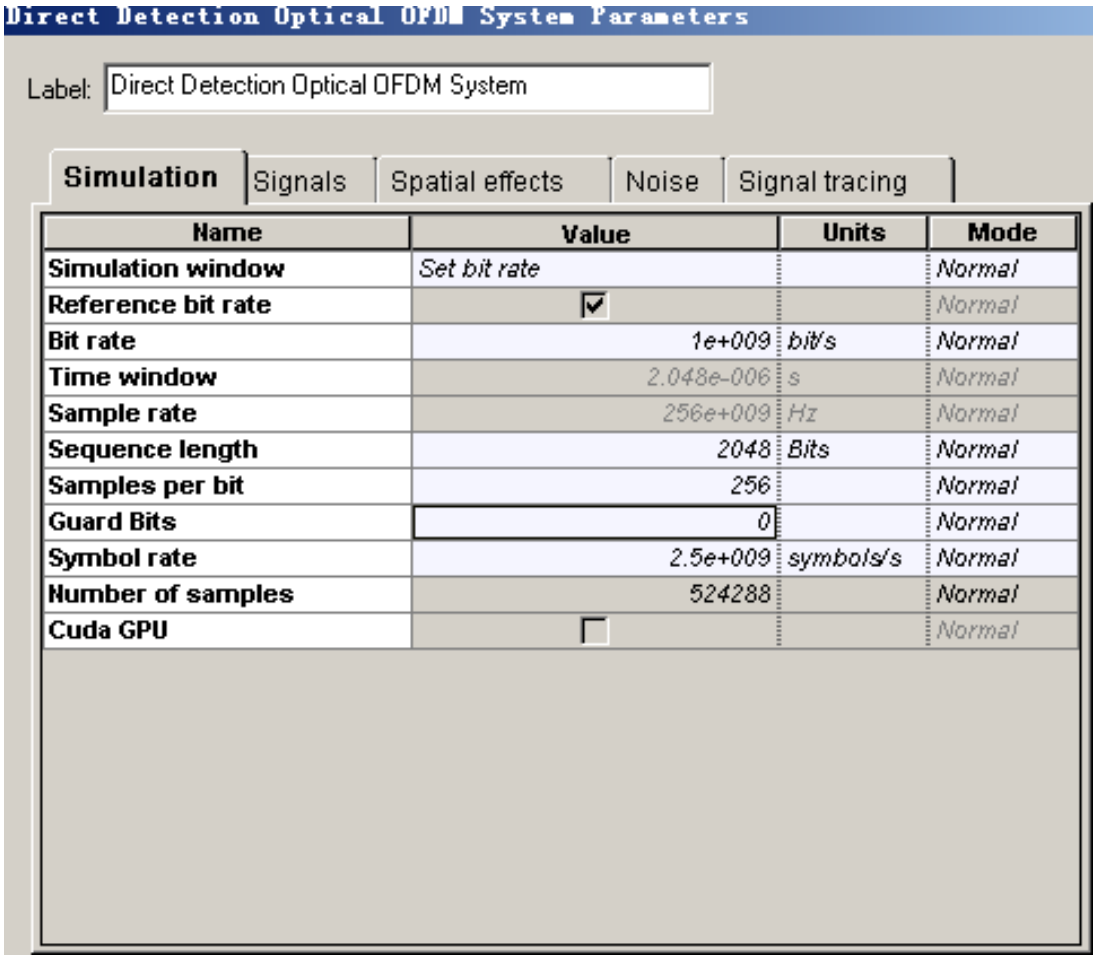

Figure 4.3: Global parameter settings of the system

PRBS Generator module: the main function of this module is to generate a binary pseudo-random bit sequence as the original input signal of the OFDM-RoF system. The sequence length is set to $2^{15} - 1$. The detailed parameter settings of the module are listed in Fig. 4.4.

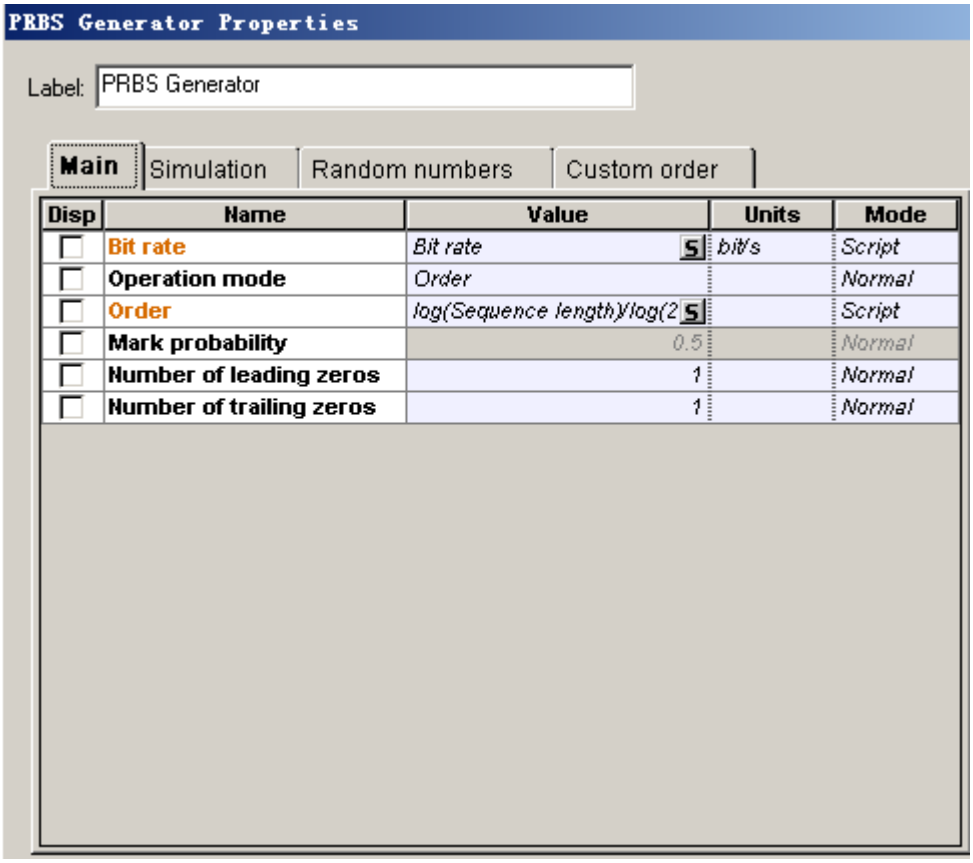

Figure 4.4: Parameter settings of PRBS Generator module

QAM Sequence Generator module: this module encodes the original binary bit sequence generated by the PRBS Generator module, which can achieve BPSK, 4-QAM, 16-QAM, 64-QAM or 256-QAM constellation by changing the parameter settings.

Subsystem module: this is the M-ary pulse generator module which generates an electrical signal for the M-QAM signal.

OFDM Modulator module: this module generates the OFDM signal. The parameter settings of this module are shown in Fig. 4.5. The number of IFFT points and subcarriers is set to 1024 and 512, respectively.

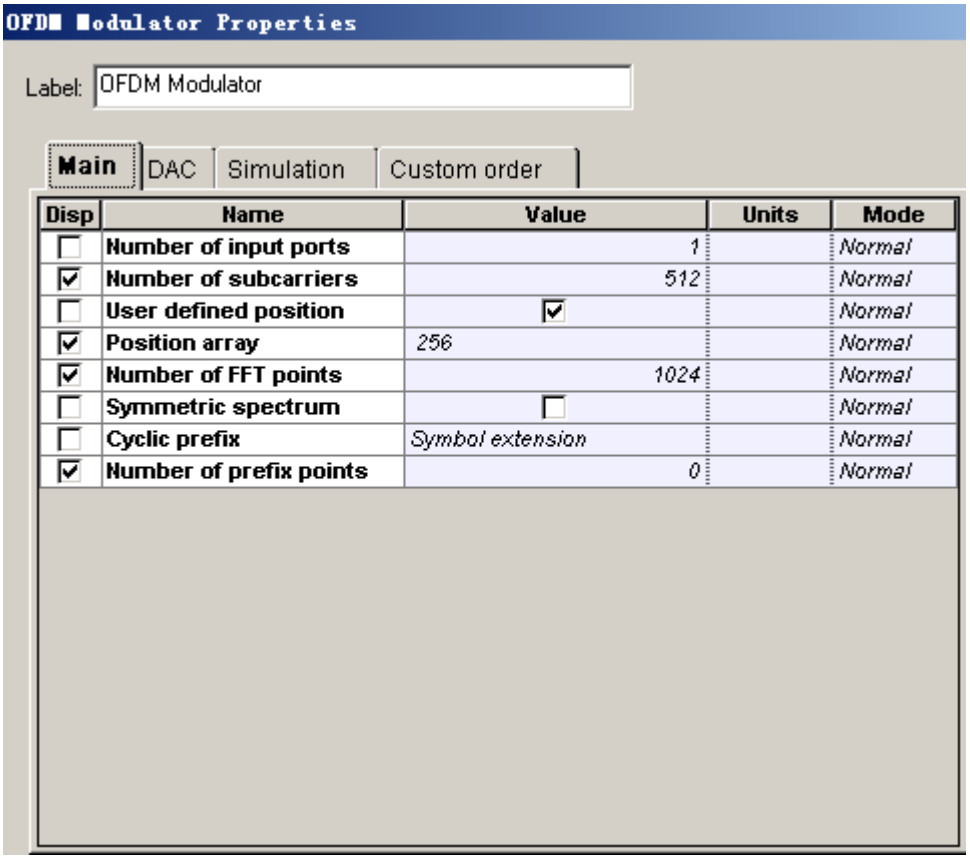

Figure 4.5: Parameter settings of OFDM Module

Quadrature Modulator module: the function of this module is to achieve I/Q modulation. The I and Q portions are multiplied by the cosine signal and the sine signal, and then added together by an adder, modulating the baseband OFDM signal onto the millimeter-wave carrier. After the module, the signal expression can be written as:

$$V_{out}(t) = G[I(t)cos(2\pi f_c + \phi_c) - Q(t)sin(2\pi f_c + \phi_c)] + b \tag{4.1}$$

Where $I(t)$ and $Q(t)$ are the input electrical signals, G is the gain, f_c is the carrier frequency, ϕ_c is the carrier phase, and b is the offset voltage.

Quadrature modulator: the I/Q modulation is carried out by the quadrature modulator. The frequency of the RF signal can be changed by setting the value of sine and cosine

waves. After the quadrature modulator module, the baseband OFDM signal is modulated on a millimeter-wave carrier.

4.3 The Optical Transmission

In the optical transmission part, MZM, Laser, fiber and photodetector are implemented in the system. The diagram of optical transmission is shown in Fig. 4.6.

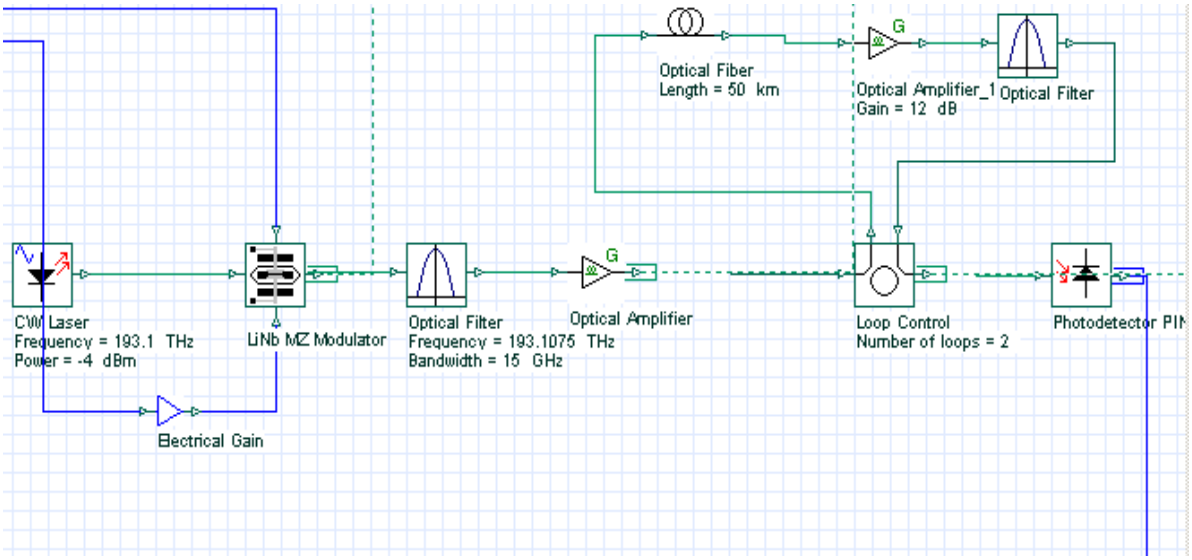

Figure 4.6: The diagram of optical transmission

MZM Module: the characters of MZM are well introduced in the last two chapter. In this MZM module, the output is given by the software in Eq. (4.2):

$$E_{out}(t) = \frac{E_{in}(t)}{10^{insertionloss/20}}[\theta e^{j\pi\frac{V_2(t)}{V_{\pi RF}}+j\pi\frac{V_{bias2}}{V_{\pi DC}}} + (1-\theta)e^{j\pi\frac{V_1(t)}{V_{\pi RF}}+j\pi\frac{V_{bias1}}{V_{\pi DC}}}] \tag{4.2}$$

where $E_{out}(t)$ is the output signal of the MZM; $E_{in}(t)$ represents the input signal; $V_1(t)$ and $V_2(t)$ represent the RF signals modulation voltage; V_{bias1} and V_{bias2} are the bias voltage 1 and 2; $V_{\pi DC}$ and $V_{\pi RF}$ are the switching bias voltage and switching RF voltage,

respectively; and θ is the extinction ratio, where $\theta = (1 - \frac{1}{\sqrt{\epsilon_r}})/2$.The MZM parameter settings is displayed in Fig. 4.7.

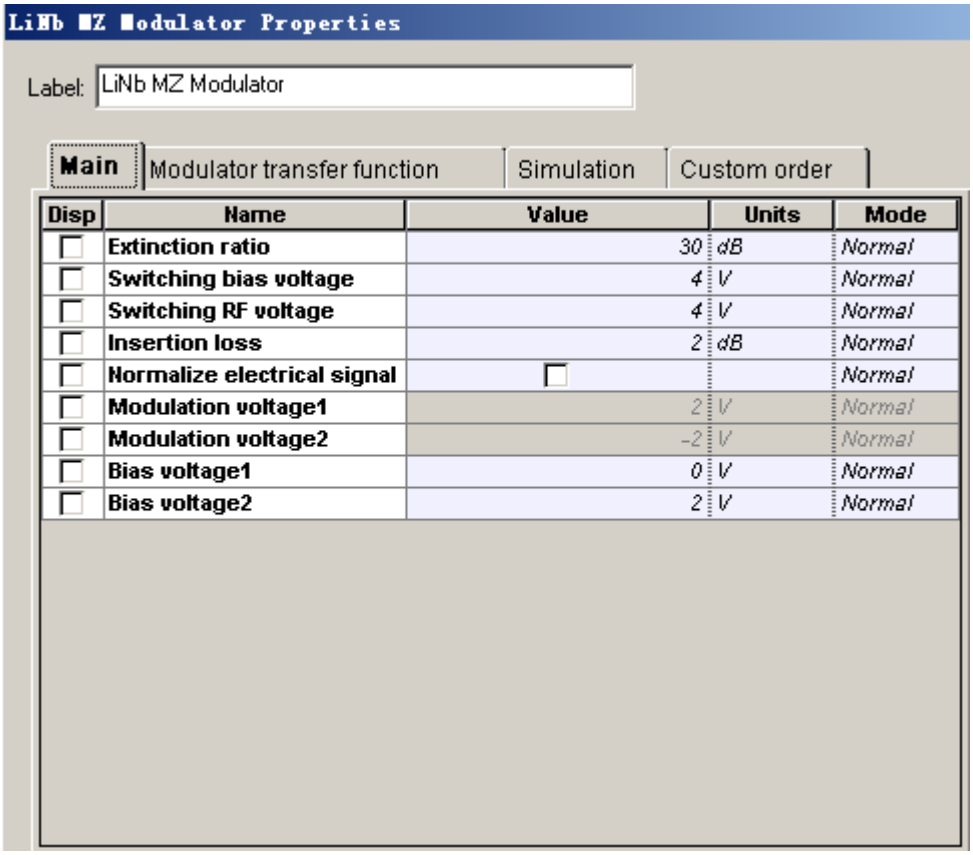

Figure 4.7: Parameter settings of the MZM

In this transmission system, the CW (continuous wave) laser is implemented. It generates continuous wavelength of light at 1552 nm (center frequency 193.1 THz), and the output power can be set to different values, as shown in Fig. 4.8.

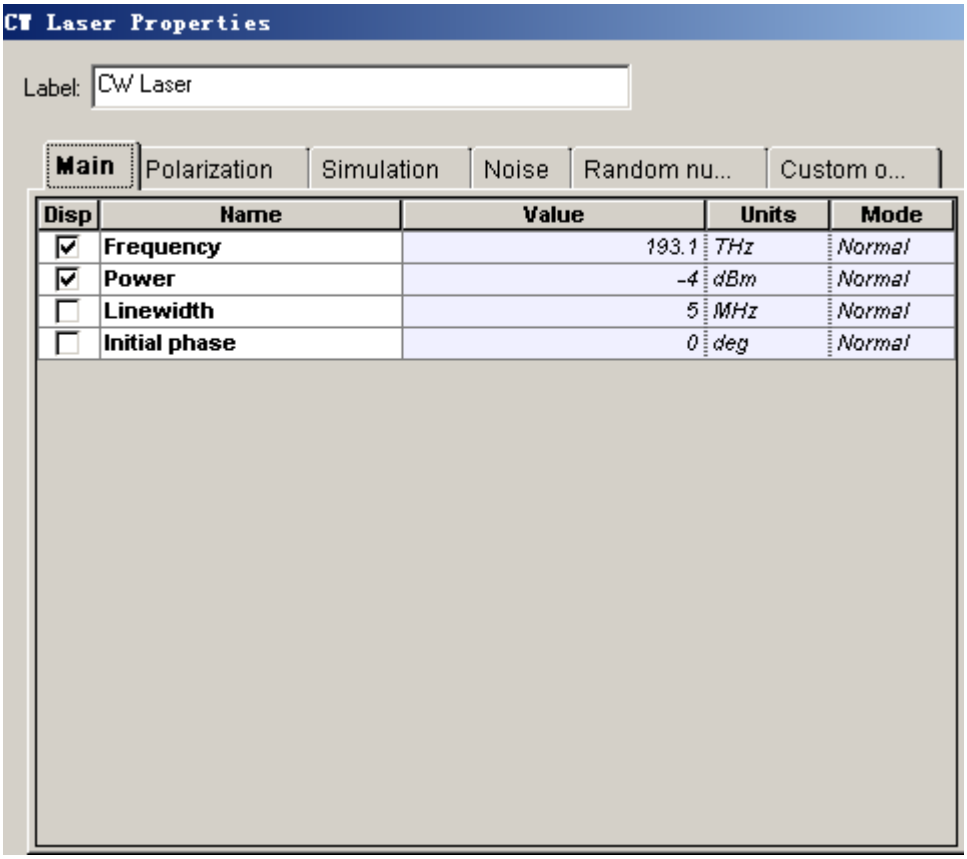

Figure 4.8: Parameter settings of the CW laser

A standard single mode fiber (SSMF) is utilized in the system, and the main parameters of the fiber are given in Fig. 4.9. The attenuation constant of SSMF is $\alpha = 0.2dB/km$; the dispersion constant is $D = 16.75\frac{ps}{nm \cdot km}$; and the polarization mode dispersion PMD is $0.5ps/\sqrt{km}$. In this simulation system, some less significant parameters of the fiber are not considered, which include the third-order dispersion coefficient, self-phase modulation, cross-phase modulation and so on.

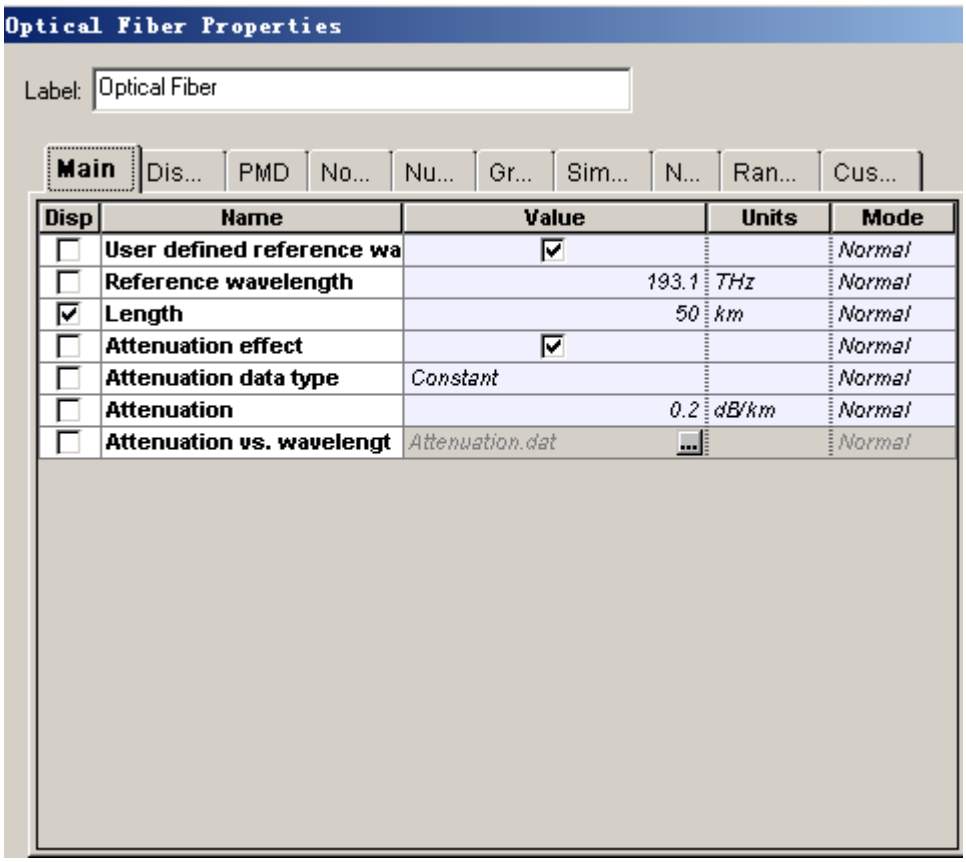

Figure 4.9: Parameter settings of the Single Mode Fiber

The role of the photodetector is to convert the received optical signal into an electrical signal. A PIN photodetector is used in the system, whose output current is determined by the following formula:

$$I_d(t) = RP_0(t) + I_n(t) \tag{4.3}$$

where $I_d(t)$ is the output current of PIN receiver; R is the responsivity of the PIN photodetector; $P_0(t)$ is the input optical power after attenuator; $I_n(t)$ is a collection of noise introduced by the current. These noises include thermal noise, PIN noise and dark noise. For simplicity, we only consider the thermal noise in the simulation. The thermal noise is set to $15 \times 10^{-24} W/Hz$, the responsivity is 1 A/W, and the dark current is 10 nA. The parameter of the PIN photodetector is shown in Fig. 4.10.

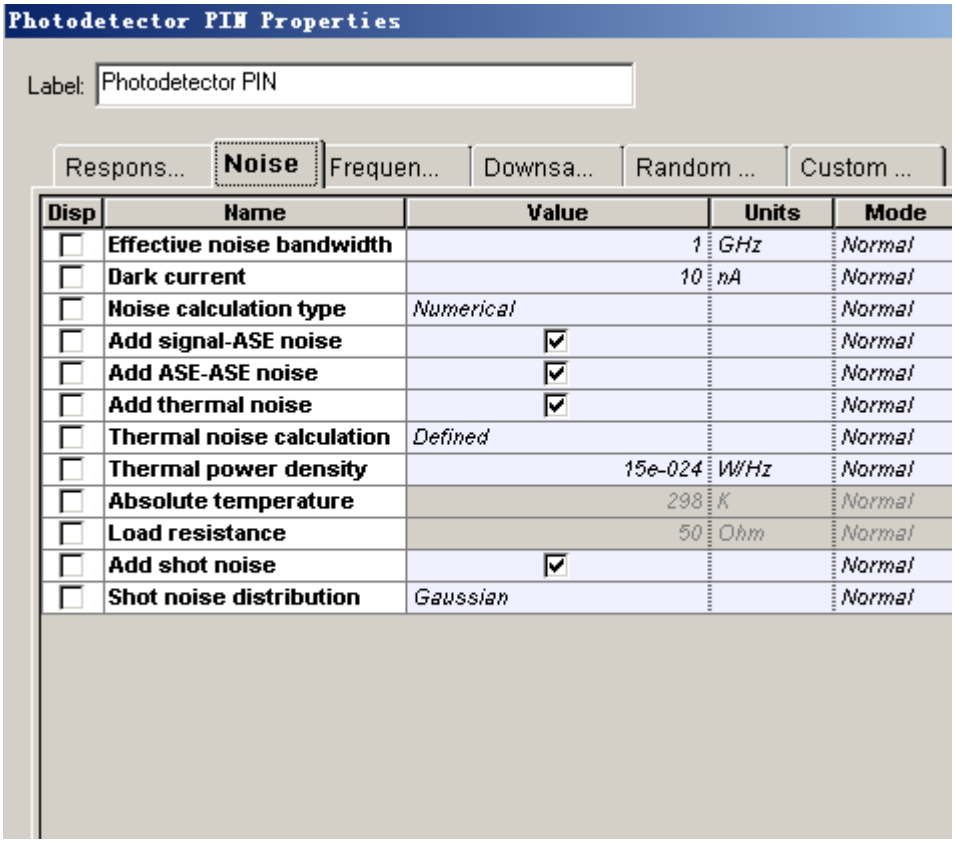

Figure 4.10: Parameter Settings of the PIN photodetector

4.4 OFDM Demodulation of the simulated system

The OFDM Demodulation of the system is quite straightforward, which is essentially the reverse operation of the modulation section. The OFDM Demodulation of the OFDM-RoF system is displayed in Fig. 4.11.

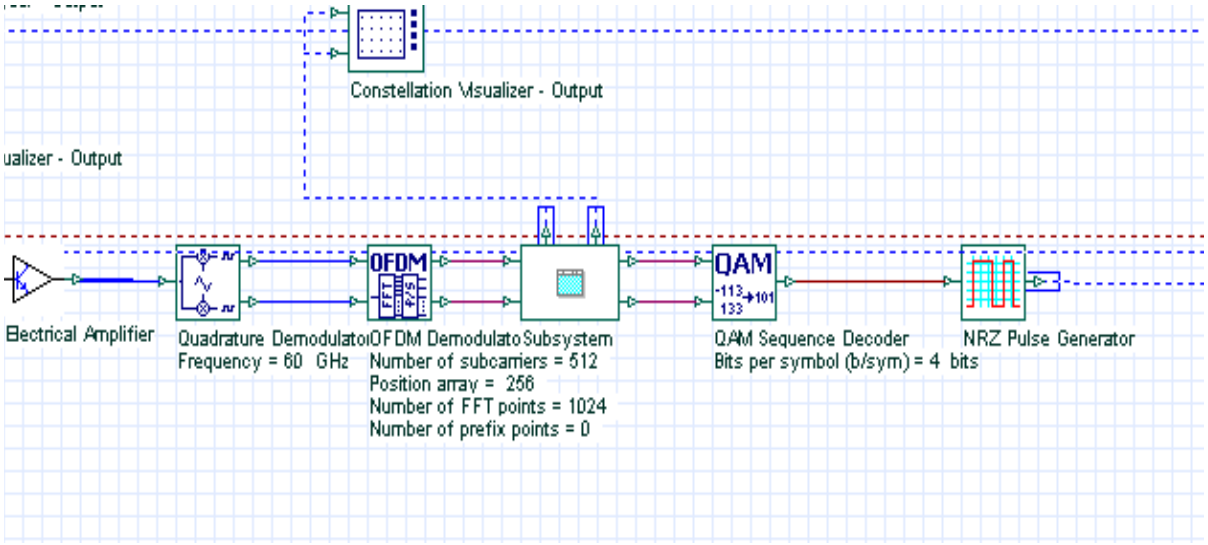

Figure 4.11: The diagram of OFDM Demodulation of the simulated system

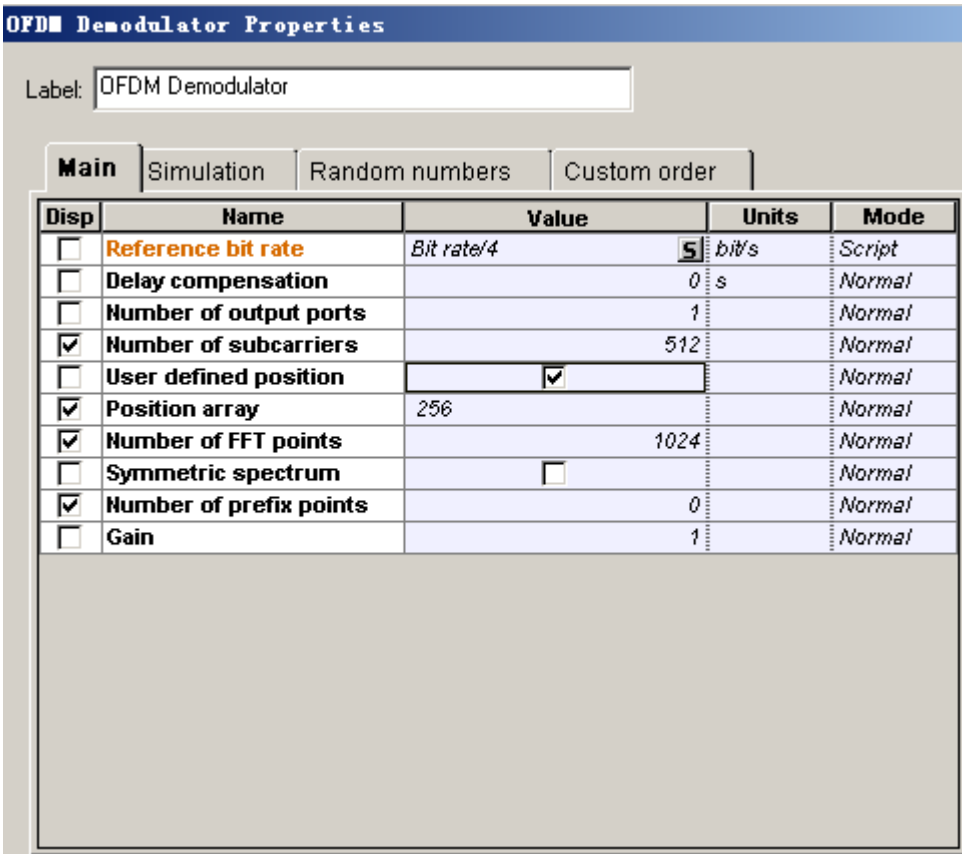

Figure 4.12: Parameter settings of OFDM Demodulator

According to Fig. 4.11, the optical signal is converted into a radio frequency signal after the PIN photodetector. The radio frequency signal is I/Q demodulated by the quadrature demodulator module to recover the baseband signal and then OFDM demodulated to obtain the binary data. Fig. 4.12 depicts the parameter settings of the OFDM Demodulator module. The BER of the optical transmission is calculated as BER_{opt}.

4.5 Co-simulation with Matlab

To calculate the end-to-end system BER performance, we co-simulate Optisystem with Matlab to achieve simulation of signal transmission over the RF channel.

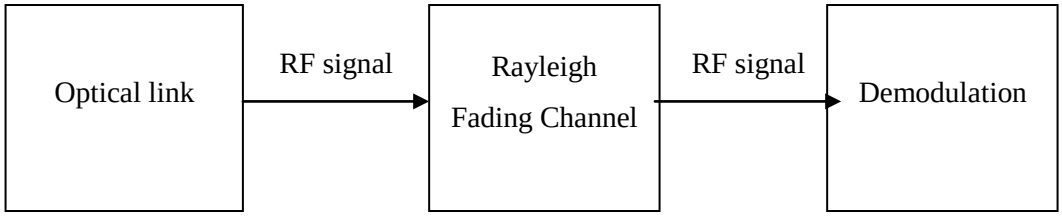

Figure 4.13: End-to-end BER calculation

As shown in Fig. 4.13, we can get a BER_{opt} of the optical link from the software Optisystem, which can be used to build a binary sequence with error by Matlab. This sequence with error is then OFDM modulated and transmitted over the Rayleigh fading channel model which is built up in last chapter. The end-to-end BER of the OFDM-RoF system is calculated by comparing the demodulated data with the original error-free sequence.

4.6 Result analysis

The BER performances of the optical link are studied under various fiber lengths and Laser powers, which are compared under different M-QAM modulations.

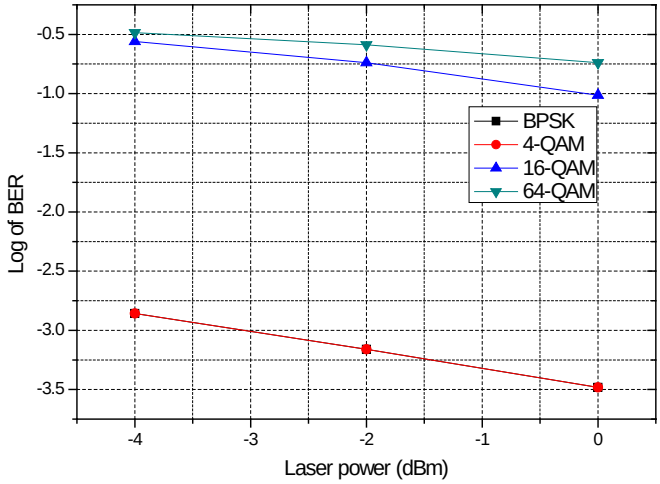

Figure 4.14: BER vs Laser power plot under different modulations (fiber length = 20 km)

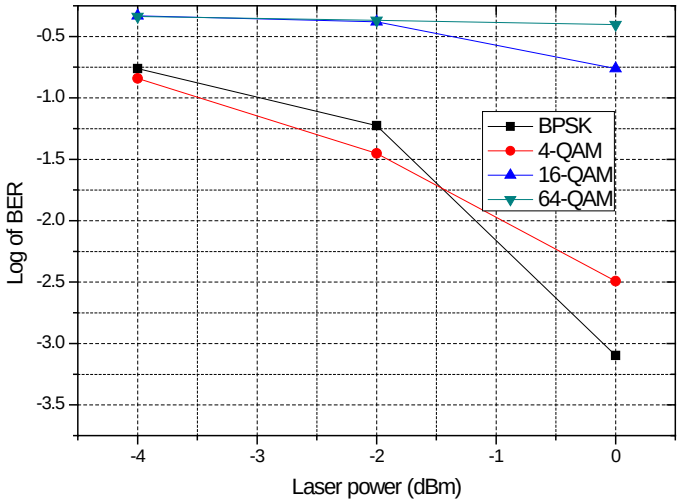

Figure 4.15: BER vs Laser power plot under different modulations (fiber length = 50 km)

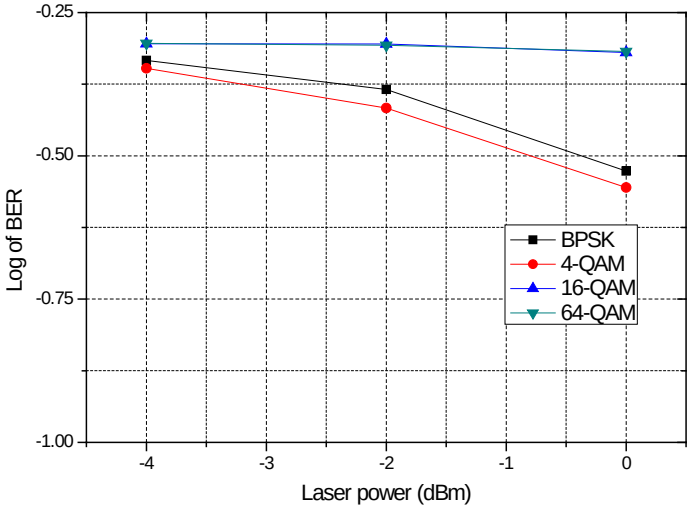

Figure 4.16: BER vs Laser power plot under different modulations (fiber length = 80 km)

Fig. 4.14, 4.15 and 4.16 display the BER vs Laser power plot under different fiber lengths, where the modulation schemes are BPSK, 4-QAM, 16-QAM and 64-QAM, respectively. As we can see from the figures, the higher the Laser power, the better the BER

performances; the BER performances of BPSK and 4-QAM are quite close to each other as they have a similar PAPR.

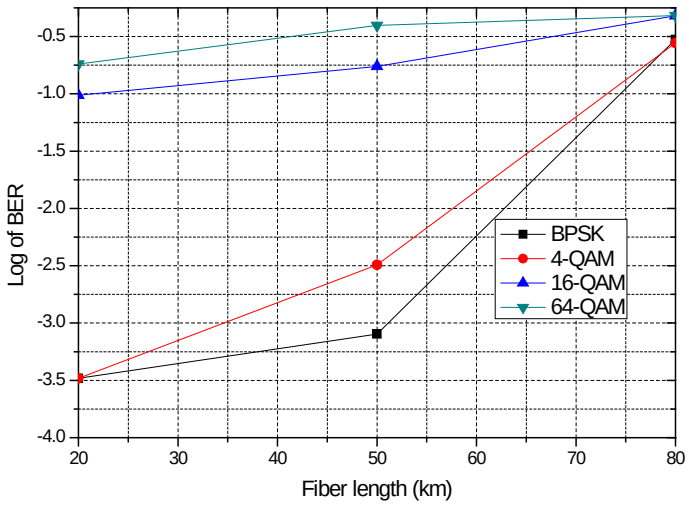

Figure 4.17: BER vs fiber length plot under different modulations (Laser power = 0 dBm)

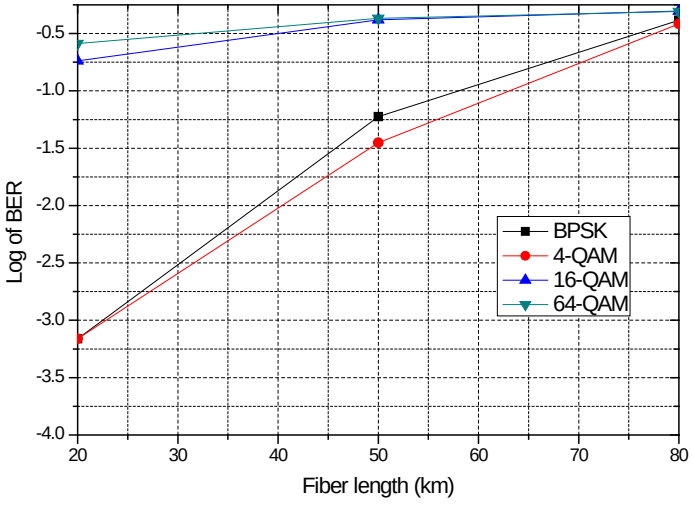

Figure 4.18: BER vs fiber length plot under different modulations (Laser power = -2 dBm)

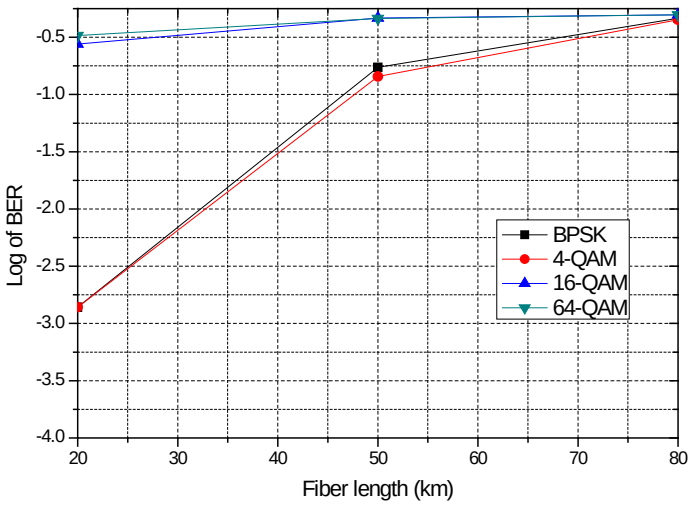

Figure 4.19: BER vs fiber length plot under different modulations (Laser power = -4 dBm)

Fig. 4.17, 4.18 and 4.19 show the BER vs fiber length plot under different Laser powers. We can draw a conclusion from the figures that the BER performances have a sudden rise at the fiber transmission distance 80 km, which means that the BER performance may have a sharp increase at a certain transmission distance. The reason for the sudden rise in the BER is that the chromatic dispersion of fiber leads to signal broadening and the probability of error detection increase dramatically after some distance of transmission.

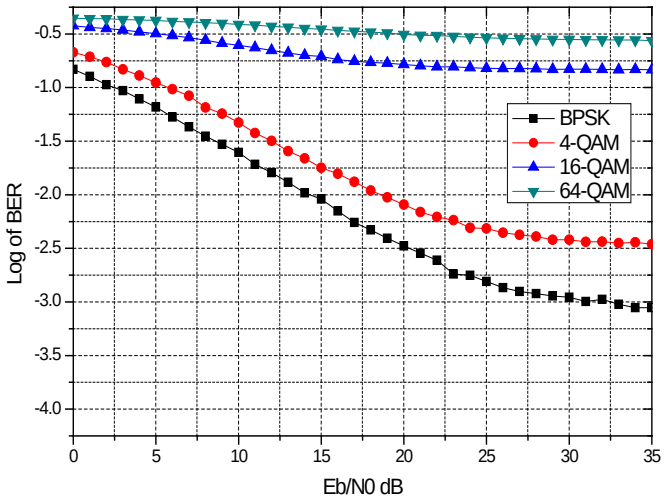

Figure 4.20: The end-to-end BER vs E_b/N_0 plot of analog RF system

Summarizing the above studies, the higher the Laser power, the better the BER performances; the BER performances of BPSK and 4-QAM are quite close to each other as they have a similar PAPR; the BER performances have a sharp increase at a certain transmission distance the chromatic dispersion of fiber.

After the optical BER simulation, we can further look into the end-to-end BER performance of the analog OFDM-RoF system by co-simulation with Matlab. Fig. 4.20 gives out the BER vs E_b/N_0 plot of the analog RF system and now we can compare the BER with the baseband system, as shown in Fig. 4.21.

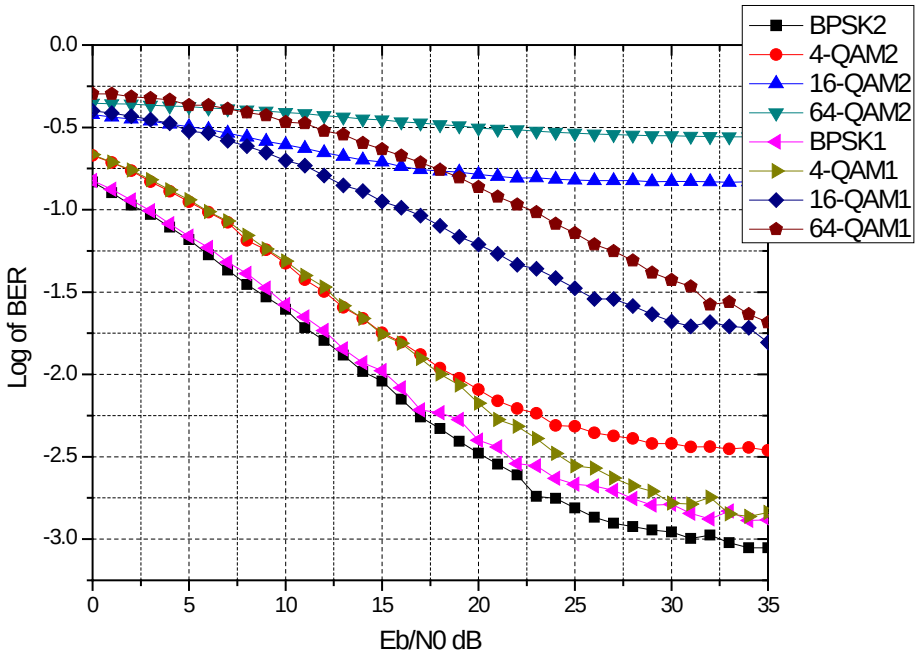

Figure 4.21: The BER comparison of the two systems

From Fig. 4.21, we can see that the BER performance of the analog RF system system is better than that of the baseband system under lower modulation level (i.e. BPSK, 4-QAM), but worse than the baseband system when modulation level is higher (i.e. 16-QAM, 64-QAM). It means that the analog RF system is more sensitive to the PAPR; it also indicates that the PAPR of the signal smaller, the BER performance better.

Chapter 5

Conclusions

The thesis has studied radio-over-fiber (RoF) that uses Orthogonal Frequency Division Multiplexing (OFDM) and the elector-optical device Mach-Zehnder modulators (MZMs), which is a promising candidate for enabling the next-generation wireless access for cost effective bandwidth provisioning. Specifically, two OFDM-RoF systems under different transmission techniques are investigated regarding their end-to-end bit-error-rate (BER) performances. The first is based on baseband OFDM-RoF while the second based on analog OFDM-RoF. By going through extensive simulation, we have observed the inferences of the nonlinear effect due to the MZM, and further tried various laser powers and fiber lengths of the optical transmission line in order to gain sufficient understanding of its performance behavior. Finally, the BER of the two systems are compared under different M-QAM modulations.

5.1 Results and discussion of the end-to-end BER of a baseband OFDM-RoF system

A baseband OFDM-RoF system is simulated and analyzed by Matlab, where the nonlinear effect of the MZM transfer function is analyzed. The end-to-end BER of the downlink system is calculated under different modulation schemes. The result analysis also compares the BER between external modulation scheme implementing the MZM and direct modulation scheme without the MZM.

After analyzing the end-to-end BER of the system, we can learn that: the BER performance of the system is worse under higher level of M-QAM modulation; MZM will cause

signal distortion due its nonlinear transfer function, and this effect is more obvious when M-QAM modulation is higher because of a higher peak-to-average power ratio (PAPR). The method of choosing MZM with a smaller V_π is proposed to reduce the effect of MZM nonlinear distortion.

5.2 Results and discussion of the end-to-end BER of an analog OFDM-RoF system

The end-to-end BER performance of an analog OFDM-RoF system is simulated and analyzed by using a commercial software Optisystem and Matlab coding. The downlink BER of the optical link of the system is studied under various laser powers and fiber transmission distances. Finally, the obtained results are further compared with that of the baseband scheme system.

We can draw several conclusions by analyzing the BER performance of the optical link of the system: the higher the laser power, the better the BER performances; the BER performances of BPSK and 4-QAM are quite close to each other as they have a similar PAPR; the BER performances have a sudden rise after a certain transmission distance because of the chromatic dispersion of fiber. Most importantly, we found the BER performance of the analog RF system is better than that of the baseband system under lower modulation level (i.e. BPSK, 4-QAM), but worse than that of the baseband system when modulation level is higher (i.e. 16-QAM, 64-QAM). It means that the analog RF system is more sensitive to the PAPR, and the BER performance is better under smaller PAPR of the signal.

References

[1] IEEE standard for telecommunications and information exchange between systems - lan/man specific requirements - part 11: Wireless medium access control (mac) and physical layer (phy) specifications: High speed physical layer in the 5 ghz band. *IEEE Std 802.11a-1999*, pages 1–102, Dec 1999.

[2] Jeffrey G Andrews, Stefano Buzzi, Wan Choi, Stephen V Hanly, Aurelie Lozano, Anthony CK Soong, and Jianzhong Charlie Zhang. What will 5g be? *Selected Areas in Communications, IEEE Journal on*, 32(6):1065–1082, 2014.

[3] Gary E Betts. Linearized modulator for suboctave-bandpass optical analog links. *Microwave Theory and Techniques, IEEE Transactions on*, 42(12):2642–2649, 1994.

[4] Vivek Ashok Bohara and See Ho Ting. Theoretical analysis of ofdm signals in nonlinear polynomial models. In *Information, Communications & Signal Processing, 2007 6th International Conference on*, pages 1–5. IEEE, 2007.

[5] Budsara Boriboon, Duang-rudee Worasucheep, Satoshi Shimizu, and Naoya Wada. Computation and experiments of 10 gb/s optical access network with long reach and a large number of subscribers. In *Electrical Engineering/Electronics, Computer, Telecommunications and Information Technology (ECTI-CON), 2015 12th International Conference on*, pages 1–6. IEEE, 2015.

[6] RS Fyath and Alhuda A Al-Mfrji. Performance evaluation of multimode fiber-based optical ofdm communication system. In *Proceedings of 1st Regional Conference of Engineering Sciences of Nahrain University, College of Engineering*, volume 11, pages 70–83, 2008.

[7] E Giacoumidis, JL Wei, XQ Jin, and JM Tang. Improved transmission performance of adaptively modulated optical ofdm signals over directly modulated dfb laser-based imdd links using adaptive cyclic prefix. *Optics express*, 16(13):9480–9494, 2008.

[8] Lajos L Hanzo, Matthias Münster, Byungcho Choi, and Thomas Keller. *OFDM and MC-CDMA for broadband multi-user communications, WLANs and broadcasting*. John Wiley & Sons, 2005.

[9] Hou-Tzu Huang, Wan-Ling Liang, Chia-Chien Wei, Chun-Ting Lin, and Sien Chi. 150-km 103-ghz direct-detection ofdm-rof system employing pilot-aided phase noise suppression. In *Optical Fiber Communications Conference and Exhibition (OFC), 2014*, pages 1–3. IEEE, 2014.

[10] AHM Islam, Rishad Ahmed Shafik, and Shawkat Ali. Comparative performance of nonlinear distortion effects in an ofdm-rof link. In *TENCON 2006. 2006 IEEE Region 10 Conference*, pages 1–4. IEEE, 2006.

[11] GL Li and PKL Yu. Optical intensity modulators for digital and analog applications. *Journal of Lightwave Technology*, 21(9):2010, 2003.

[12] Chong-U Lim, Yizhuo Yang, and Ampalavanapillai Nirmalathas. High performance fiber-radio link: Digitized radio-over-fiber. In *Communications and Photonics Conference (ACP), 2012 Asia*, pages 1–3. IEEE, 2012.

[13] Christina Lim, Ampalavanapillai Nirmalathas, Yizhuo Yang, Dalma Novak, and Rod Waterhouse. Radio-over-fiber systems. In *Asia Communications and Photonics*, pages 76321S–76321S. International Society for Optics and Photonics, 2009.

[14] Simon Litsyn. *Peak power control in multicarrier communications*. Cambridge University Press, 2007.

[15] Jia-Ming Liu. *Photonic devices*. Cambridge University Press, 2005.

[16] Yanir London and Dan Sadot. Nonlinear effects mitigation in coherent optical ofdm system in presence of high peak power. *Lightwave Technology, Journal of*, 29(21):3275–3281, 2011.

[17] Ampalavanapillai Nirmalathas, Prasanna Gamage, Christina Lim, Dalma Novak, Rodney Waterhouse, et al. Digitized radio-over-fiber technologies for converged optical wireless access network. *Lightwave Technology, Journal of*, 28(16):2366–2375, 2010.

[18] Linghui Rao, Xiaoqiang Sun, Wei Li, and Dexiu Huang. Ofdm-rof system and performance analysis of signal transmission. In *2006 Optics Valley of China International Symposium on Optoelectronics*, 2006.

[19] Marvin K Simon and Mohamed-Slim Alouini. *Digital communication over fading channels*, volume 95. John Wiley & Sons, 2005.

[20] GH Smith, D Novak, and Zabir Ahmed. Technique for optical ssb generation to overcome dispersion penalties in fibre-radio systems. *Electronics Letters*, 33(1):74–75, 1997.

[21] Tuan Nguyen Van and Tung Ton That Thanh. Study on performance of digitized radio over fiber (rof) system using edfa and coherent receiver. In *Computing and Communication Technologies, Research, Innovation, and Vision for the Future (RIVF), 2013 IEEE RIVF International Conference on*, pages 91–96. IEEE, 2013.

[22] Mathuranathan Viswanathan. Simulation of digital communication systems using matlab [ebook]. *Published: Feb*, 18:2013, 2013.

[23] Chia-Chien Wei, Chun-Ting Lin, Ming-I Chao, Wen Jiang Jr, and Chun-Hung Ho. Long-reach 26.54-gbps ofdm rof system at 60 ghz over 100-km fiber and 3-m wireless transmission employing phase noise compensation and bit-loading algorithms. In *European Conference and Exposition on Optical Communications*, pages We–7. Optical Society of America, 2011.

[24] Yizhuo Yang. Investigation on digitized rf transport over fiber. 2011.

[25] Yizhuo Yang, Christina Lim, and Ampalavanapillai Nirmalathas. Digitized rf-over-fiber technique as an efficient solution for wideband wireless ofdm delivery. In *Optical Fiber Communication Conference*, pages OTu2H–6. Optical Society of America, 2012.

[26] Xingwen Yi, William Shieh, and Yiran Ma. Phase noise effects on high spectral efficiency coherent optical ofdm transmission. *Journal of Lightwave Technology*, 26(10):1309–1316, 2008.

[27] Jianjun Yu, Ming-Fang Huang, Dayou Qian, Lin Chen, and Gee-Kung Chang. Centralized lightwave wdm-pon employing 16-qam intensity modulated ofdm downstream and ook modulated upstream signals. *Photonics Technology Letters, IEEE*, 20(18):1545–1547, 2008.